ORNL/Sub--83-43346/02

DE89 014789

Breakdown Mechanisms of Al_2O_3, Cr_2O_3 and SiO_2 Scales in $H_2/H_2O/H_2S$ Environments

January 31, 1989

Final Report Volume I

Prepared by

G. M. Kim and G. H. Meier

Department of Materials Science and Engineering
University of Pittsburgh
Pittsburgh, PA 15261

under

Subcontract Number 19X-43346-C

Program Manager: R. R. Judkins

for

OAK RIDGE NATIONAL LABORATORY
Oak Ridge, Tennessee 37831
operated by
MARTIN MARIETTA ENERGY SYSTEMS, INC.
for the
U.S. DEPARTMENT OF ENERGY
under Contract No. DE-AC05-84OR21400

Breakdown Mechanisms of Al_2O_3, Cr_2O_3 and SiO_2 Scales in $H_2/H_2O/H_2S$ Environments

Gil M. Kim and Gerald H. Meier

ABSTRACT

The breakdown mechanisms of preformed oxide scales, Cr_2O_3, Al_2O_3 and SiO_2, have been studied at low oxygen and high sulfur potentials in the temperature range 550 to 950°C.

For Cr_2O_3 on Ni-30Cr, sulfur penetration occurs through thin areas in the Cr_2O_3 scale. These thinner areas were formed over voids formed during preoxidation because the voids act as chromium diffusion barriers. Internal sulfides form at the rim of the voids where the chromium activity is high. The filling of voids by the sulfides and the progressive formation of sulfides through the scale establish sulfide rich channels which are easy paths for cation transport. The breakdown occurs once the channels are introduced. The first sulfides to form on Fe-25Cr and Co-30Cr were observed at the scale/gas interface as the result of Fe or Co transport through the Cr_2O_3 scale.

Alumina scales on Fe-18Cr-6Al-1Hf were broken down by crack formation. Addition of Hf to the alloy improved scale adherence and extended the time to breakdown. However, sulfur reacts with metallic iron on the surface and HfO_2 extending through the Al_2O_3 scale to form iron sulfides and hafnium rich sulfides, respectively. These sulfides provide easy paths for inward diffusion of sulfur ions and outward diffusion of base metal ions to form internal sulfides at craters around Hf rich phases, and external sulfides at the scale/gas interface, respectively. Additions of Ti to Fe-18Cr-6Al provided improved scale adherence without introducing continuous paths through the oxide scales. These scales were even more resistant than those on the Hf-containing alloys when exposed in high sulfur potential atmospheres. These results also extended to long term cyclic sulfidation/oxidation experiments and simulated syngas exposures. Pure alumina scales were never formed on Ni-18Cr-6Al and Co-18Cr-6Al alloys and the NiCrAl alloy underwent catastrophic corrosion in most sulfidation/oxidation exposures.

For SiO_2 on Ni-20Si, although porosity can form at the scale/gas interface due to the high vapor pressures of SiS and SiO, the formation of a thin layer of vitreous silica and good scale adherence provide better resistance to sulfur penetration than do Cr_2O_3 and Al_2O_3. The SiO_2 scales formed on Fe-20Si and Co-20Si were not as protective as those formed on Ni-20Si.

Key Words: Fe-18Cr-6Al, Ni-18Cr-6Al, Co-18Cr-6Al, Fe-20Si, Co-20Si, Ni-20Si, Ni-30Cr, Fe-25Cr, Co-30Cr, Scale Breakdown, Oxygen-Active Elements, Sulfidation/Oxidation

INTRODUCTION

Current high temperature alloys and coatings are designed to resist high temperature degradation in highly oxidizing atmospheres by the formation of a protective oxide film (usually Cr_2O_3, Al_2O_3, or SiO_2) by selective oxidation. However, in some processes (e.g. coal gasification) the alloys and coatings are exposed to environments with low oxygen potentials and high potentials of other reactants such as sulfur and carbon.[1,2] Exposure to such environments often leads to formation of reaction products, such as sulfides or carbides, which are less protective than oxides even in atmospheres where Cr_2O_3, Al_2O_3, or SiO_2 are thermodynamically stable. Preformed films of Cr_2O_3, Al_2O_3 or SiO_2 should continue to grow in these atmospheres and improve corrosion resistance until the scales break down due to the formation of less protective reaction products. The length of time a given oxide remains protective is expected to depend on its thickness and integrity, the composition of the underlying alloy, the atmosphere composition, and temperature.[3]

The objective of this research is directed toward studying the mechanisms by which preformed oxide layers are degraded in the high P_{S_2} and low P_{O_2} environments.

"Research sponsored by the U.S. Department of Energy, AR&TD Fossil Energy Materials Program, DOE/FE AA 15 10 10 0, Work Breakdown Structure Element PITT-3"

BACKGROUND

Breakdown of Chromia Scales

Degradation of preformed Cr_2O_3 scales in sulfur-bearing gases has been studied by several investigators.[3-9] Such degradation can occur by diffusive processes or through mechanical defects in the scale. Diffusive breakdown can occur if metal cations, such as Ni, Co and Fe, diffuse through the oxide scale to the scale/gas interface and subsequently are sulfidized, or sulfur diffuses through the oxide scale to the substrate and forms internal sulfides at the scale/alloy interface. Mechanical breakdown has been proposed[9] as the result of the continuous cracking of oxides scales which has been shown to occur in many systems.[10]

Natesan[1] investigated the sulfidation/oxidation of preformed Cr_2O_3 scales on pure chromium. The predominant Cr sulfide at the scale/gas interface was observed by the use of SEM without any evidence of sulfur transport into or through the oxide scale. He concluded that the formation of the sulfide crystals on the external surface was largely controlled by chromium diffusion through the oxide scale. Stirling[7] studied the breakdown of the Cr_2O_3 scales on Fe-25Cr in $H_2/H_2O/H_2S$ gas mixtures at 900°C. This involved the initial nucleation of chromium-rich sulfides at the scale/gas interface, at sites corresponding to short-circuit diffusion paths for metal ions. Inward transport of sulfur toward the scale/alloy interface occurs beneath the external sulfides, leading to the establishment of sulfide channels within the scale. These channels provide easy diffusion paths for metallic ions to the surface and allow the formation of sulfides richer in iron. Huang, et al.[11] studied the stability of the chromium oxide scales formed on Fe-30Cr and Co-30Cr. The outward transport of iron ions through the chromium oxide scale on Fe-Cr was dominant and led to the formation of alloyed

chromium sulfides on the surface of preoxidized specimens, even when the gas composition fell in the chromium oxide stable region of the Cr-S-O system. No significant transport of Co ions through the chromium oxide scale on Co-Cr was observed. The chromium oxide scale on Co-30Cr was more stable than that on Fe-30Cr.

Breakdown of Alumina Scales

Alumina scales are generally more protective than chromia scales in sulfur bearing atmospheres.[5,6,14-16] Mari, et al.[15] found that the sulfidation behavior of Fe-Cr-Al alloys after preoxidation to form Al_2O_3 was dependent on the potential of sulfidizing species in the sulfidation atmosphere. In pure sulfur, at lower pressure, a layered sulfide scale containing chromium and iron sulfides initially developed as a result of the diffusion of metal ions through the Al_2O_3 scale. On the other hand, sulfide nucleated and grew beneath the Al_2O_3 when the preoxidized alloy was exposed in H_2/H_2S at atmospheric pressure. This implies the possible penetration of gas molecules through physical defects, such as cracks in the oxide scale. Huang, et al[11,12,17] observed significant amounts of isothermal acoustic emission (indicating cracking) from aluminum oxide scales formed on Fe-Cr-Al alloys when grown in environments containing only oxygen. When the sulfur activity at the scale/gas interface was increased the adherence of the Al_2O_3 was improved and the amount of isothermal cracking drastically reduced due to the change in diffusion mechanisms from predominant inward oxygen diffusion to predominant outward aluminum ion diffusion through the oxide scale. However, Smeggil, et al.[18] proposed that sulfur present in the alloy even at low concentration (<100 ppm) segregates to and weakens the scale/metal interface, thereby promoting scale exfoliation. Kim, et al[19] recently reported that sulfur segregates to grain boundaries of Cr_2O_3 and Al_2O_3 scales. In addition they also

found that the presence of sulfur in Cr_2O_3 scales tends to damage scale adhesion. A detailed explanation for the effect of sulfur on the adhesion of oxide scales has not yet been determined. Further study in this area is particularly needed.

Huang et al.[17] studied the effect of yttrium and hafnium on the breakdown of Al_2O_3 scales formed in coal gasification environments. They reported that the order of resistance to cracking in a simple oxidation environment was Fe-Cr-Al-Hf > Fe-Cr-Al-Y > Fe-Cr-Al, which paralleled the order of resistance to sulfidation attack after preoxidation. This suggests that the breakdown of Al_2O_3 can be initiated by the transport of H_2S through cracks in the oxide scale. Stott, et al[6,14] first reported the adverse effect of yttrium on the degradation of preformed oxide scales (Cr_2O_3 or Al_2O_3) in a sulfur-bearing environment for Fe-Cr-Al and Fe-Cr alloys exposed at 750°C in $H_2/H_2O/H_2S$ gas mixtures. Preoxidation to develop Al_2O_3 on Fe-Cr-Al and similar alloys containing yttrium provides a very significant improvement in corrosion resistance on subsequent exposure to equilibrated $H_2/H_2O/H_2S$ gases at 750°C. Breakdown of the preformed oxide scales on the Cr_2O_3-forming alloys occurred at a much earlier stage than on the Al_2O_3-forming alloys. It was also observed that some sulfide nodules developed relatively rapidly on the yttrium containing alloys. Sulfide nodules were usually formed over the area where second phase yttrium-rich precipitates (YFe_9) were located at or near the surface. It was concluded that the oxidation of the yttrium-rich phase results in an increase in localized Fe ion activity near the scale/gas interface. Also, oxidation of the yttrium-rich phase to Y_2O_3 is associated with a 9.1% increase in volume which could create further localized scale defects. The addition of reactive elements such as Y and Hf to the alloys improves the scale adherence and integrity during high temperature oxidation. However, their presence in the alloys may influence the degradation of the preformed oxide scale upon exposure to sulfur-bearing environments.

Breakdown of Silica Scales

Some SiO_2 forming alloys have been observed to oxidize slower than typical Cr_3O_3 - and Al_2O_3 - forming alloys as a result of a SiO_2 film.[20-22] When some alloys (Ni-20Si and Fe-20Si) were exposed to sulfur-bearing gases ($H_2/H_2O/H_2S$), these alloys were very effective upon relatively short term exposures. However, there was some evidence of growth of small Fe-sulfides at the scale/gas interface of Fe-20Si when exposed to sulfur-bearing gases.[23] The long term stability of preformed SiO_2 scales on these alloys must be investigated.

EXPERIMENTAL

The alloys listed in Table 1 were prepared from 99.9% pure raw materials by arc melting in argon and drop casting in a chilled copper mold, 9.5 x 25.4 x 152.4 mm in size. The ingots were homogenized at 1100°C for 100 hours in an argon gas stream. Test specimens, approximately 12 x 9 x 2 mm in size, were ground on all surfaces through 600 grit on wet silicon carbide papers and ultrasonically cleaned in methanol.

Most sulfidation and sulfidation/oxidation experiments were carried out at 950°C in H_2/H_2S and $H_2/H_2O/H_2S$ mixtures with $p_{S_2} = 10^{-6.1}$ and $p_{O_2} = 10^{-18.7}$ atm, respectively. The position of this composition relative to the phase boundaries for the individual metal-sulfur-oxygen systems of the various alloy components is indicated for reference in Figure 1. Limited experiments were performed at other gas compositions and temperatures. Preoxidation was generally performed in H_2/H_2O mixtures with the same p_{O_2} as the $H_2/H_2O/H_2S$ mixture. The $H_2/H_2S/H_2O$ gas mixtures were prepared by mixing 2.02% H_2S in H_2, H_2 and Ar gases using precision flow meters. Water vapor was supplied to the gas mixture by bubbling the argon through a water bath at constant temperature to produce a saturated gas of the desired water vapor content. The total gas flow rate was 200

cc/min. To prevent condensation loss of water vapor the inlet and outlet to the furnace were heated using electrical heating tape. A platinum coated alumina honeycomb was placed in the reaction chamber to ensure equilibrium in the gas mixture. The experimental apparatus allowed specimens to be preoxidized in H_2/H_2O or air and subsequently exposed to equilibrated $H_2/H_2S/H_2O$ gas mixtures at the reaction temperature without opening the reaction chamber. Specimens were held in the reaction chamber outside the furnace, while the system was flushed with nitrogen gas for 20 minutes. Following this the $H_2/H_2S/H_2O$ or H_2/H_2O gas mixture was introduced. After equilibrium of the gas mixture was obtained, the specimen was moved to the hot zone by a magnet. At the end of an experiment, the specimen was pulled out to the cold zone. The temperature of the furnace was held constant within $\pm 2^oC$ during a run. After sulfidation/oxidation experiments and prior to preoxidation experiments in sulfur-free environments, the apparatus was baked out at higher temperature than the reaction temperature for more than 24 hours to minimize sulfur contamination in the reaction chamber.

Cyclic sulfidation/oxidation tests after preoxidation were conducted to study the effects of the integrity and adhesion of the oxide scale upon exposure to sulfur-bearing gases. All specimens were preoxidized for 30 minutes at 950^oC to provide preformed oxide scales on the alloy surfaces prior to cyclic sulfidaton/oxidation. Preoxidized specimens were exposed to a $H_2/H_2S/H_2O$ gas mixture for 4 hours at 950^oC, removed from the furnace, weighed, and reinserted for the next 4 hours followed by cooling to room temperature.

In order to examine the long term stability of the various alloys, specimens of Ni-30Cr, Fe-18Cr-6Al-1Hf, Fe-18Cr-6Al-1Ti, Fe-20Si, and Ni-20Si were coated with gasifier slag (from Illinois #6 coal) and then exposed to syngas (32.4% H_2,

48.6% CO, 10.8% CO_2, 0.66% H_2S, 6.9% H_2O and 0.55% HCl), which is a very aggressive environment, for 160 hours at 550°C at Lockheed Palo Alto Research Laboratory.

Most of the reaction products were identified by X-ray diffraction (XRD) techniques. The surface morphology and cross section of the scales were examined by scanning electron microscopy (SEM) with energy dispersive x-ray analysis (EDX) and wave length dispersive analysis (WDX). The scale/alloy interfaces were studied by obtaining spalled oxide or mechanically removing layers using a Sebastian adherence test machine. Both the underside of a given scale and the alloy substrate were examined. Prior to examination in the SEM, specimens were coated with palladium by evaporation to prevent charging effects and to increase contrast.

RESULTS AND DISCUSSON

Cr_2O_3 - FORMING ALLOYS

A. Simple Oxidation

Specimens were oxidized isothermally for a week at 950°C in flowing air. The weights of the specimens were continuously recorded during oxidation using a Cahn 2000 microbalance. The results are shown in Figure 2. All alloys formed a Cr_2O_3 layer after a week of oxidation at 950°C. The relative growth rates of the scales were in the order of Fe-25Cr > Co-30Cr > Ni-30Cr.

B. Sulfidation - Oxidation

In these experiments, all specimens were preoxidized for 30 minutes at 950°C to provide preformed oxide scales on the alloy surface prior to exposure to sulfur-bearing gases unless otherwise specified. Table 2 shows how the preoxidation treatment can improve the degradation resistance to subsequent sulfidation/oxidation in terms of weight gains. The relative resistance of the preformed Cr_2O_3 scales to sulfidation/oxidation atmospheres was in the order of Co-30Cr > Fe-25Cr > Ni-30Cr.

Specimens of Ni-30Cr which were oxidized in a H_2/H_2O gas mixture at 950°C for 30 minutes and subsequently exposed to a $H_2/H_2O/H_2S$ gas mixture at 950°C for 5, 10 and 20 minutes are shown in Figures 3, 4 and 5, respectively. The scale/alloy interfaces were examined by pulling the oxide scale from the alloy substrate using a Sebastian adherence test machine. No evidence of external sulfide formation on the oxide scale was observed after 5 minutes of sulfidation/oxidation, Figure 3. External sulfides at the scale/gas interface and internal sulfides at the scale/alloy interface were observed after 10 minutes of sulfidation/oxidation, Figure 4. In the early stages of sulfidation/oxidation, both external and internal sulfides were mainly chromium sulfides, however, the external sulfides were alloyed with a small amount of Ni. External chromium sulfides were covered by a thin layer of chromium oxide and internal chromium sulfides were found to be attached to the underside of the oxide scale. The distribution of internal sulfides was similar to that of voids, which had already formed in the alloy substrate during preoxidation (see below). Chromium sulfides were found in discrete nodules and in ring-shaped formations indicating a relationship to the rims of the voids. The rims on the underside of the oxide scale appeared to grow together to form internal sulfide particles, whose sizes were similar to those of the voids in the alloy substrate. This suggests that sulfur penetrates the Cr_2O_3 scale over the voids and nucleates internal sulfides preferentially at the the rims of voids where the activity of chromium is highest (if chromium evaporation in the voids is negligible). The newly formed internal sulfides around the voids appeared to grow and eventually fill the voids. In order to check the relationship between the external sulfides and internal sulfides the specimen shown in Figure 4, was taper-polished, resulting in the removal of the external sulfides, shown in (a) of Figure 6. An arrow in this micrograph indicates a

site where an external sulfide was located. The site is concave and contains sulfur as shown by EDX. These concave dimples have been observed after the preoxidation of Ni-30Cr, shown in Figure 7. Therefore, the penetration of sulfur appeared to occur preferentially through the oxide scale over the voids and eventually produce sulfide-rich channels through the preformed oxide scale. As the reaction progressed, the external sulfides became enriched in nickel and formed nickel sulfides on top of the initially formed chromium sulfides, as shown in Figure 5. These nickel sulfides are thermodynamically stable at the scale/gas interface. Both (b) and (c) of Figure 5 correspond to micrographs of the underside of the oxide scale and the alloy substrate which was severely degraded at this stage.

Different Scale Thickness Development During Preoxidation

After 30 minutes of preoxidation in an H_2/H_2O mixture at 950°C, α-Cr_2O_3 forms on Ni-30Cr. The oxide layer is relatively smooth and shows no indication of cracking or spalling. However, a considerable number of voids are formed at the oxide scale/alloy interface, as shown in Figure 7. The voids act as diffusion barriers for the transport of chromium from the alloy if the transport of chromium from the alloy by vaporization through the voids is not significant. In this case, the thickness of the oxide scale over the voids is less than that away from the voids. Chromium transport, both through the voids and across the scale/alloy interface, and the subsequent development of differential scale thickness are illustrated in Figure 8. At any time during the oxidation period, the rate of evaporation of chromium from the alloy surface of the voids at a given temperature can be calculated from published chromium vapor pressures[24,25] and the Langmuir equation

$$R_{Cr}(\text{alloy}) = a_{Cr} \times P \times (M/2\pi RT)^{1/2}, \text{ g/cm}^2\text{.sec} \qquad (1)$$

where R_{Cr} is the rate of chromium vaporization from the alloy, a_{Cr} is the activity

of chromium at the alloy surface, P is the vapor pressure of pure chromium, M is the atomic weight of chromium, R is the gas constant and T is absolute temperature.

Recently, Azhar[26] developed computer models to calculate chromium concentration profiles in Ni-30Cr during oxidation. By utilizing these results for the Cr concentration gradient in Ni-30Cr after 30 minutes of preoxidation at 950°C, the flux of chromium to the scale/alloy interface can be calculated by using Fick's first law.

$$J_{Ni\text{-}30Cr} = - D^{Cr}_{Ni\text{-}30Cr} \times (\Delta C/\Delta X),\ g/cm^2.sec \qquad (2)$$

where $J_{Ni\text{-}30Cr}$ is the flux of chromium, $D^{Cr}_{Ni\text{-}30Cr}$ is the diffusivity of chromium in Ni-30Cr, ΔC is the concentration difference and ΔX is the distance.

The flux of Cr through the Cr_2O_3 scale after 30 minutes of oxidation at 950°C may also be expressed by[27]

$$J_{Cr_2O_3} = - C_{Cr} \times (K_p/X),\ g/cm^2.sec \qquad (3)$$

where $J_{Cr_2O_3}$ is the flux of chromium through the Cr_2O_3 scale in $g/cm^2.sec$, C_{Cr} is the concentration of chromium in the oxide scale in g/cm^3, K_p is the parabolic rate constant in cm^2/sec and X is the oxide scale thickness in cm.

Calculated values of the rate of chromium vaporization across the voids, the flux of chromium at the scale/alloy interface away from the voids and the flux of chromium through the oxide scale after 30 minutes of oxidation at 950°C are $5.7 \times 10^{-10} g/cm^2.sec$, $4 \times 10^{-8}\ g/cm^2.sec$ and $3.5 \times 10^{-8}\ g/cm^2.sec$, respectively. The chromium flux at the scale/alloy interface away from the voids and the flux through the oxide scale are comparable and two orders of magnitude greater than the calculated rate of chromium vaporization across the voids at 950°C. These results are consistent with the thinner oxide scale over the voids, shown in Figure 7. When voids are formed at the oxide/alloy interface, they may act as

concentration sites for thermal stresses induced during cooling. This may lead to crack formation in and spalling of the oxide scale. However, acoustic emission studies of the oxidation of Ni-30Cr at 950°C indicated that cracking and/or spalling of the Cr_2O_3 layer did not occur. A number of authors proposed gaseous transport through microchannels which were developed through the oxide scale by the so called 'dissociation mechanism'. However, the porous oxide at the oxide scale/alloy interface, which is characteristic of the oxide formed by the dissociation mechanism,[28] was not observed after 30 minutes of oxidation at 950°C. Since the possibility of gas phase diffusion through cracks and/or spalling of the scale and microchannels of the oxide scale is ruled out, the protectiveness of the scale appears to depend only on the solid-state diffusion of reactive species. In other words, if degradation occurs by the diffusion of reactive species, such as sulfur or metallic elements, through the preformed oxide scale, differences in scale thickness will play an important role in the degradation of the scale.

Upon exposure to sulfur-bearing gases, sulfur arrives at the scale/void interface and moves to the rim of the voids, probably by surface diffusion. The chromium activity at the rim of the voids is high because chromium evaporation is negligible at 950°C. Internal sulfides, mainly chromium sulfides, nucleate at the triple point of the scale, the void and the alloy substrate. Figure 9 shows the concentration profile of sulfur across Ni-30Cr which was preoxidized in a H_2/H_2O gas mixture for 30 minutes and subsequently exposed to a $H_2/H_2O/H_2S$ gas mixture for 4 hours at 700°C. The formation of external sulfides is predominant where voids exist, as shown in (a) of Figure 9. A line scan of sulfur in (b) of Figure 9 shows the sharp increase of sulfur concentration at the rim of the voids. This suggests that sulfur is concentrated at the rim of the voids prior to the formation of external sulfide. In other words, sulfur penetrates preferentially through Cr_2O_3

over the voids and moves to the rim of the voids, where internal sulfides form. This result is consistent with the formation of ring-shape internal sulfides, which were observed on the underside of the Cr_2O_3 layer, shown in Figure 6. Sulfide nucleation and subsequent growth in the voids are not restricted and the sulfides continue to grow from the underside of the scale and progressively fill the voids. At the same time, chromium moving outward through chromium sulfides and sulfur moving inward through the Cr_2O_3 scale react at the oxide/sulfide interface and progressively form sulfide-rich channels, which are easy paths for metal transport, because the chromium diffusion through sulfide is several orders of magnitude faster than that through chromium oxide.[28] As the internal sulfides fill the voids at the scale/alloy interface, newly formed sulfides in the voids and sulfide rich channels through the oxide scale enhance mainly chromium transport. Consequently, chromium reaches the scale/gas interface and reacts with sulfur from the gas phase. Chromium sulfide is not thermodynamically stable at the scale/gas interface. However, nickel also diffuses out through the sulfide-rich channels and results in a gradual decrease in the activity of chromium at the scale/gas interface, accompanied by an increase in the activity of nickel. Eventually the activities of chromium and nickel at the scale/gas interface approach values for which alloyed chromium sulfide is stable and the Cr_2O_3 scale stops growing, whereas the alloyed chromium sulfide begins to grow upon it.[5,26] A thin layer of Cr_2O_3 may form on the alloyed chromium sulfide by reaction (4).

$$2\,(CrS) + 3/2\,O_2(g) = Cr_2O_3(s) + S_2(g) \qquad (4)$$

where (CrS) indicates CrS dissolved in a NiS-CrS solution. Thin layers of Cr_2O_3 were observed to cover the sulfides during the early stages of the reaction. As the sulfidation/oxidation continues, nickel diffuses out through the sulfide-rich channels to form virtually pure nickel sulfides on top of the alloyed chromium

sulfide. The formation of nickel sulfides, which are thermodynamically stable at the scale/gas interface, accelerates the degradation processes because these sulfides are liquid at 950°C and breakdown of the oxide scale occurs. The proposed mechanism of breakdown of preformed Cr_2O_3 scale on Ni-30Cr by sulfur-bearing gases is illustrated schematically in Figure 10. The resistance of preformed Cr_2O_3 scales on Ni-30Cr to sulfur-bearing gases was improved by high temperature preoxidation, such as at 1150°C. (Table 3) Preoxidation at higher temperatuare provides a more protective Cr_2O_3 layer mainly due to increased scale thickness. Even though larger voids are formed at the scale/gas interface, the thickness of the oxide scale over the voids is comparable to that away from the voids because transport of chromium vapor through the voids becomes comparable to the flux of chromium through the oxide scale at the higher temperature.

Figure 11 shows Fe-25Cr which was preoxidixed in a H_2/H_2O gas mixture at 950°C for 5 hours and subsequently exposed to a $H_2/H_2O/H_2S$ gas mixture for 10 minutes at the same temperature. The sulfides were observed at the scale/gas interface but not at the scale/alloy interface. Figure 12 shows sequential growth of external sulfide at the same temperature. It was evident that the size and the amount of external sulfides at the scale/gas interface increased with time. Thus, in contrast to the breakdown of Cr_2O_3 scales on Ni-30Cr, the formation of sulfide on the preformed Cr_2O_3 scale of Fe-25Cr was initiated at the scale/alloy interface. This observation has been reported by Stirling[7] and by Perkins.[2]. This can be explained in that the diffusivity of Fe through the Cr_2O_3 is higher than that of Ni[2] and the Cr_2O_3 layer formed on Fe-25 Cr is less pure. This is shown in Figure 13. The Cr_2O_3 scale at the scale/gas interface contains a significant amount of iron, shown in EDX(A) and the one at the scale/alloy interface does not, shown in EDX(B).

Figure 14 shows Co-30Cr which was preoxidized in a H_2/H_2O gas mixture at 950°C for 30 minutes and subsequently exposed to a $H_2/H_2O/H_2S$ gas mixture for 10 and 20 minutes at the same temperature. The extent of sulfidation on Co-30Cr was not significant compared to that on the Ni-30Cr and Fe-25Cr alloys. However, a few chromium sulfides were observed at the scale/gas interface. The improved behavior of Cr_2O_3 on Co-30Cr is believed to result from slower transport of Co through Cr_2O_3, relative to Fe transport,[2] and to the lower thermodynamic stability of Co sulfides compared to those of Fe and Ni. Ultimately, the breakdown of the scales was initiated by the formation of Cr sulfides at the scale/alloy interface.

Al_2O_3 - Forming Alloys

A. Simple Oxidation

Specimens were oxidized isothermally for a week at 950°C in flowing air. The weights of the specimens were continuously recorded during oxidation using a Cahn 2000 microbalance. The results are shown in Figure 15. All Fe-base alloys formed a Al_2O_3 layer after a week of oxidation at 950°C. Both Ni- and Co-base alloys, however, formed an external Cr_2O_3 layer with internal Al_2O_3 rather than a continuous external Al_2O_3 layer. The relative growth rates of the scales were in the order of Co-18Cr-6Al-1Hf > Ni-18Cr-6Al-1Hf > Fe-18Cr-6Al, Fe-18Cr-6Al-1Hf.

B.Sulfidation/Oxidation

Fe-18Cr-6Al-1Hf was preoxidized in a H_2/H_2O gas mixture at 950°C for 30 minutes and subsequently exposed to a $H_2/H_2S/H_2O$ gas mixture for 4 hours at the same temperature, Figure 16. Small white particles, identified as iron sulfides, were observed around HfO_2 in the Al_2O_3 scale. These particles were formed from metallic Fe remaining from oxidation of $HfFe_2$ during preoxidation. Comparatively large particles, identified as chromium sulfides and showing some oxygen in WDX analysis, were located beside the small sulfide particles. It is concluded that

sulfides form initially by sulfidation of metallic Fe around HfO_2 and that as the sulfidation/oxidation continues, the small iron sulfides are outgrown by chromium sulfides, covered by a thin layer of chromium oxide. Figure 17 shows an Al_2O_3 scale pulled from the substrate to reveal the scale/alloy interface. The external oxide layer appeared to be protective except for the formation of iron sulfides around hafnium-rich regions. The underside of the Al_2O_3 scale, shown in (b) of Figure 17, revealed both sulfides and oxides. The oxide particles were mainly Al_2O_3 and hafnium oxides which had not been transformed to sulfides, and the sulfide particles were hafnium-rich sulfides, as shown in (b) of Figure 17. The preformation of the Al_2O_3 scale on Fe-18Cr-6Al-1Hf produced craters around hafnium oxide pegs, shown in (b) of Figure 18. Upon sulfidation/oxidation, the hafnium oxide pegs were reacted to hafnium-rich sulfides and the craters formed during the preoxidation were filled by these sulfides. Except for these sulfides, the oxide scale/alloy interface was relatively smooth and appeared to be intact. Figure 19 shows a further developed stage of the sulfidation-oxidation in the same $H_2/H_2S/H_2O$ gas mixture at 950°C. The outermost sulfide layer was iron sulfide and beneath this layer a chromium sulfide layer was observed. Figure 20 shows the spalling of the oxide scale around a Hf-rich phase in the alloy substrate. From the results of the sulfide formation and the oxide scale failure around HfO_2, it can be concluded that the sulfidation of Fe-18Cr-6Al-1Hf is closely related to the existence of Hf in the alloy.

For comparison, Fe-18Cr-6Al was exposed to the same environment as the Fe-18Cr-6Al-1Hf, Figure 21. The numbers of external sulfide nodules were fewer but the sizes were significantly larger compared to those on Fe-18Cr-6Al-1Hf. The Al_2O_3 scale adherence on Fe-18Cr-6Al was observed to be very poor, as shown in Figure 21. In addition, cracking of the alumina scales was detected by acoustic

emission measurements during preoxidation in air with the cracking being more extensive when water vapor was added in the gas phase. Therefore, it is concluded that the large sulfides in Figure 21 are the result of cracking of the alumina scale during exposure. These results are consistent with those of Huang, et al[16] who reported the cracking of oxide scales formed on Fe-Cr-Al in a $H_2/H_2S/H_2O$ gas mixture at 900°C. Therefore, it is seen that Hf additions to Fe-Cr-Al improve its overall resistance to high P_{S_2} gases by improving the mechanical integrity of the scales but that the presence of Hf-rich regions in the scale provide the sites for eventual breakdown. Apparently, the development of hafnium-rich sulfides through the oxide scale provided easier diffusion paths both inward for sulfur and outward for metallic components. Penetration of sulfur through the sulfides leads to the formation of internal hafnium-rich sulfides to fill the craters which were formed during preoxidation. Outward transport of chromium and iron through the hafnium-rich sulfides resulted in the formation of chromium and iron sulfides on the external oxide surface. Furthermore, since the oxidation of hafnium increases the volume by 40%, growth stresses may have accumulated in the hafnium oxide pegs during the preoxidation, even though the stresses were not high enough to induce cracking or spalling during preoxidation. Upon sulfidation-oxidation, more growth stresses accumulate around the hafnium rich regions, leading to spalling of the scale, as shown in Figure 20. The deleterious effect of hafnium on the sulfidation-oxidation of Fe-18Cr-6Al-1Hf is further substantiated by higher temperature preoxidation. With preoxidation at higher temperature (1150°C), the sulfidation attack was worse. The examination of the preoxidized Fe-18Cr-6Al-1Hf revealed more hafnium oxides in the Al_2O_3 scale and voids at the scale/alloy interface. Acoustic emission tests were employed to check for cracking or spalling of the oxide scale during cooling to the sulfidation-oxidation temperature (950°C) from

the preoxidation temperature (1150°C). The results showed negligible cracking and/or spalling in the scale. It is proposed that the major part of the sulfidation attack may be attributed to the transformation of HfO_2 pegs to hafnium-rich sulfides, which are easy paths for diffusion of sulfur and metallic components through the Al_2O_3 scale and, secondly, the void formation around HfO_2 pegs in the alloy substrate. The proposed mechanism of breakdown of preformed Al_2O_3 scale by sulfur-bearing gases is schematically illustrated in Figure 22. Similar effects of Y on scale breakdown of Cr_2O_3 and Al_2O_3 have been reported previously[6,14,29]. Thus an oxygen active element which can improve adherence without providing transport paths through the scale should be preferable to Hf or Y. The results of cyclic oxidation tests Figure 23 indicated that Ti additions to FeCrAl produced such adherence effects but without the formation of Ti-rich oxides in the scale.[30] The Ti additions also produced substantial improvements in the resistance to scale breakdown over those produced by Hf (Figure 24).

Figures 25 and 26 show Co-18Cr-6Al-1Hf and Ni-18Cr-6Al-1Hf, respectively, which were preoxidized in H_2/H_2O at 950°C for 30 minutes and subsequently exposed to a $H_2/H_2S/H_2O$ gas mixture for 4 hours at the same temperature. There was no significant formation of Co-sulfide on the CoCrAl but the NiCrAl was covered with Ni-sulfides. In fact, the extent of degradation of the NiCrAl was comparable to that of Ni-30Cr exposed under the same condition which is consistent with the inability of the NiCrAl to form a protective alumina scale with only 6 wt% Al in the alloy.

The protectiveness of the preformed alumina scales depends greatly on their integrity and adhesion, which is degraded due to the build-up of stresses in the oxide scale. A cyclic sulfidation/oxidation test after preoxidation was conducted to study these effects. All specimens were preoxidized for 30 minutes at 950°C to

provide preformed oxide scales on the alloy surface prior to the cyclic sulfidation/oxidation test. Preoxidized specimens were exposed to a $H_2/H_2S/H_2O$ gas mixture for 4 hours at 950°C, removed from the furnace, weighed, and reinserted for the next 4 hours of sulfidation/oxidation. Each cycle consisted of isothermal sulfidation/oxidation at 950°C for 4 hours followed by cooling to room temperature. The results are shown in Figure 27. Differences in the rates of sulfidation/oxidation were significant depending on the types of the alloys. For Fe-base alloys, the addition of oxygen active elements (Hf, and especially Ti) improved the resistance to cyclic sulfidation/oxidation. Even though both Co- and Ni-base alloys formed external Cr_2O_3 scales after preoxidation, the Co-base alloy exhibited fairly good resistance to sulfidation/oxidation, better than Fe-base alloys. The Ni-base alloy showed the worst resistance in sulfur-bearing gases.

The long term stability of Fe-Cr-Al-Ti, Fe-Cr-Al-Hf, and Co-Cr-Al-Hf was evaluated in a simulated syngas exposure at Lockheed Palo Alto Research Laboratory. Specimens were coated with gasifier slag (from Illinois #6 coal) and exposed to syngas (32.4% H_2, 48.6% Co, 10.8% CO_2, 0.66% H_2S, 6.9% H_2O and 0.55% HCl) for a total of 995 hours at 550°C. Typical cross-sections of each of the alloys are shown in Figure 28. The corrosion products were complex mixtures of oxides and sulfides which incorporated some chlorine. However, the Ti-modified FeCrAl showed the best resistance among the three alloys.

SiO_2 - Forming Alloys

A. Simple Oxidation

Specimens of each alloy were oxidized isothermally for one week at 950°C in flowing air. The results are shown in Figure 29. Generally, the growth rate of the oxide scale on the alloys was slow compared to typical Al_2O_3- and Cr_2O_3-forming alloys. Ni-20Si exhibited the best oxidation resistance among the alloys. The

surface of the oxide scale formed on Ni-20Si after a week of oxidation in air was examined by SEM and exhibited only the polishing marks present on the specimen prior to oxidation. Furthermore, the oxide scale was too thin to be detectable with conventional X-ray diffraction analysis. Figure 30 is a transmission electron micrograph of the SiO_2 layer formed over the single phase (δ) and two-phase (δ + Ni_3Si_2) regions with two selected area electron diffraction patterns. For this analysis Ni-20Si specimens 3 mm in diameter and 80 um in thickness were oxidized in air for one hour at 950°C. The alloy substrate was removed by jet electropolishing leaving a thin layer of SiO_2. The oxide layer consisted of a clear vitreous silica layer along with transient oxide islands (Ni_2SiO_4), identified by selected area diffraction patterns in the figure. It is apparent that a vitreous silica layer formed over the δ + Ni_3Si_2 constituent and transient oxides formed over the δ-phases of the alloy (lower silicon content). The growth rate of vitreous scales is significantly less than that of polycrystalline scale probably due to the absence of grain boundary transport.[12] It is concluded that a thin layer of vitreous silica formed on Ni-20Si is very effective during isothermal oxidation. A vitreous SiO_2 layer was also reported to form on Fe-20Si alloys[7] along with a significant amount of Fe_2O_3. It is believed that the larger weight gain for Fe-20Si and Co-20Si, as compared to Ni-20Si, is the result of the formation of Fe_2O_3 and CoO, respectively.

B. Sulfidation - Oxidation

M-Si alloys were exposed to a sulfidizing atmosphere (2% H_2S in H_2) for 4 hours at 950°C. The weight changes for these experiments are as follows:

Ni-20Si---------- -4.53 mg/cm^2

Fe-20Si---------- -0.16 mg/cm^2

Co-20Si---------- -0.16 mg/cm^2

The sulfidation morphologies are presented in Figure 31. Significant amounts of porosity in the surface of Ni-20Si and deep penetration of these pores into the alloy substrate were observed, (a) of Figure 31. The formation of porosity and the penetration into the alloy appear to be related to the weight loss (-4.53 mg/cm^2) and suggest the evaporation of some components in the alloy because cracking or spalling was not observed. Figure 32 illustrates the vapor species diagram for the Si-S system at 950°C. The sulfur potential applied was $P_{S_2} = 10^{-6.1}$ atm. The vapor pressure of SiS is extremely high at this sulfur potential, on the order of 0.1 atm. One can conclude that the development of porosity in the alloy was mainly due to the vaporization of SiS. Surprisingly, nickel sulfide, which is thermodynamically stable in this H_2/H_2S gas mixture, was not observed and instead, deep penetration of porosity into the alloy was observed. The existence of a SiO_2 layer was confirmed by WDX and EDX analyses on the surface even though porosity existed. In the sulfidation of Ni-20Si trace amounts of oxygen-bearing impurities in the component gases may play an important role in the formation of the oxide scale. An oxygen partial pressure of about 10^{-26} atm at 950°C, which is high enough to form a SiO_2 layer, has been estimated previously.[31] It is believed that initially a thin SiO_2 layer formed during the heat-up period of the specimen, because at lower temperatures the vapor pressure of SiS is quite low (e.g., $P_{SiS} = 2.7 \times 10^{-3}$ atm at 700°C). Once a SiO_2 layer formed, this layer was unlikely to be permeable to sulfur at 950°C and the vaporization of SiS and SiO at the gas/SiO_2 interface may have occurred by following reactions

$$SiO_2(s) + 1/2\ S_2(g) = SiS(g) + O_2(g) \quad (5)$$

or

$$SiO_2(s) = SiO(g) + 1/2\ O_2(g) \quad (6)$$

By assuming unit activity of SiO_2 in reactions (5) and (6) and an oxygen partial pressure of about 10^{-26} atm due to trace amounts of oxygen-bearing impurities in the gases[31] the vapor pressures of SiS and SiO at 950°C were calculated to be $P_{SiS} = 1.34 \times 10^{-5}$ atm and $P_{SiO} = 1.09 \times 10^{-8}$ atm. Thus, the SiO_2 layer appeared to be degraded mainly by the vaporization of SiS. Therefore, two competing processes occur resulting in a substrate penetrated by tortuous porosity. First, the initially formed SiO_2 layer is being reduced in thickness by evolution of SiS. Secondly, as Si is selectively oxidized to reheal this scale, counterdiffusion of Ni occurs into the substrate from these localized regions. The net result is the formation of pores which extend into the substrate as the above processes are repeated. The mechanism of degradation of Ni-20Si by H_2/H_2S mixtures at 950°C is schematically illustrated in Figure 33. Though degradation of Fe-20Si and Co-20Si alloys in a H_2/H_2S gas mixture was much less than that of typical Cr_2O_3 - and Al_2O_3 alloys,[1,2] both alloys suffered weight loss after sulfidation. However, the magnitudes of the weight losses were much less than that for Ni-20Si. The reason for these differences have not been determined.

The effect of preoxidation on the sulfidation/oxidation of Ni-20Si, Co-20Si and Fe-20Si was studied in sulfur-bearing gases. Specimens were preoxidized for 30 minutes at 950°C in a H_2/H_2O gas mixture ($P_{S_2} = 1.95 \times 10^{-19}$ atm) to provide preformed oxide scales prior to exposure to a $H_2/H_2O/H_2S$ gas mixture ($P_{S_2} = 8 \times 10^{-7}$, $P_{O_2} = 1.95 \times 10^{-19}$ atm) unless otherwise specified. While the SiO_2 scales formed on Ni-20Si and Fe-20Si were very effective in sulfur-bearing gases, that on Co-20Si was not.

The corresponding corrosion morphology of Ni-20Si is presented in Figure 34. Sulfidation was not observed and the appearance was similar to that of the preoxidized specimen. Wrinkles, shown in (a), were formed during SEM observation

because the bombardment of electrons on the very thin oxide scale deformed the scale easily. Actually the oxide scale was smooth and flat. No degradation was observed at the scale/gas or scale/alloy interfaces unless cracks existed in the starting material. A few nickel sulfide nodules were found along cracks, which existed in the alloy before exposure to the sulfur-bearing gases, Figure 32. The formation of sulfide nodules can be explained as follows; in the confined region within a crack, the local oxygen potential in the gas phase equals the local oxygen potential in the thin layer of oxide along the crack. In this case sulfide formation is possible if the local oxygen potential is too low to form an oxide layer and the local sulfur potential is high enough to form nickel sulfide, which is liquid at the reaction temperature. In $H_2/H_2S/H_2O$ gas mixtures, P_{H_2S} in cracks or pores in a preformed oxide layer is approximately constant.[32] Local depletion of oxygen at the tip of the crack and the high sulfur potential of a $H_2/H_2S/H_2O$ gas mixture leads to sulfide formation. These liquid sulfides move to the alloy surface under the influence of capillarity forces. In conclusion, the SiO_2 scale formed on Ni-20Si is very effective in sulfur-bearing gases unless cracks exist. The proposed mechanism of the breakdown of preformed SiO_2 scales by sulfur-bearing gases is schematically illustrated in Figure 36.

Figure 37 shows Fe-20Si which was preoxidized in a H_2/H_2O gas mixture at 700°C for 30 minutes and subsequently exposed to a $H_2/H_2O/H_2S$ gas mixture for 4 hours at the same temperature. Small particles of iron sulfide were observed at the scale/gas interface but not at the scale/alloy interface. Overall sulfidation attack was not significant. The long term stability of these alloys in high-P_{S_2}, low-P_{O_2} atmospheres still must be determined as considerable outward diffusion of Fe through the SiO_2 scales has been observed for exposures in pure O_2.[20] This

transport may eventually result in scale breakdown initiating at the scale/gas interface.

Co-20Si exhibited the worst sulfidation/oxidation resistance among the alloys. Figure 38 shows Co-20Si which was preoxidized in a H_2/H_2O gas mixture at 950°C for 30 minutes and subsequently exposed to a $H_2/H_2O/H_2S$ gas mixture for 4 hours at the same temperature. It is apparent that the SiO_2 scale formed on Co-20Si was not pure after preoxidation and outward diffusion of Co through the SiO_2 scale was relatively fast. This may result in scale breakdown initiating at the scale/gas interface. Since the eutectic temperature of Co-Co_4S_3 is 877°C,[33] cobalt sulfide forms liquid at 950°C. This accelerates the breakdown of preformed oxide scales.

The protectiveness of the preformed oxide scale also depends on its integrity and adhesion, which is degraded due to the build-up of stresses in the oxide scale. Cyclic sulfidation/oxidation tests after preoxidation were conducted to study the effects of the integrity and adhesion of the oxide scales upon exposure to sulfur-bearing gases. Each cycle consisted of isothermal sulfidation/oxidation at 950°C for 4 hours followed by cooling to room temperature. The results are shown in Figure 39. While differences in the weight changes after cyclic sulfidation/oxidation were not significant, the corresponding corrosion morphologies showed substantial differences, Figure 40. While Ni-20Si maintained good resistance to cyclic sulfidation/oxidation after 44 hours, Fe-20Si and Co-20Si showed some degradation. Whenever specimens were cooled down, oxide scales which contained small particles of base metal sulfide separated from the alloy substrate. However, new oxide scales containing sulfide particles reformed upon heating to reaction temperature. As the above processes were repeated, a number of oxide layers with sulfide particles were developed, (b) and (c) of Figure 40.

Therefore, Fe- and Co-base alloys formed successive oxide layers containing base metal sulfides as a result of scale separation.

For the examination of long term stability of SiO_2-forming alloys, specimens of Ni-20Si and Fe-20Si alloys were coated with gasifier slag (from Illinois #6 coal) and then exposed to syngas (32.4% H_2, 48.6% CO, 10.8% CO_2, 0.66% H_2S, 6.9% H_2O and 0.55% HCl) for 160 hours at 550°C at Lockheed Palo Alto Laboratory. The results for Ni-20Si and Fe-20Si alloys are shown in Figures 41 and 42, respectively. Fe-20Si exhibited severe degradation in the syngas exposure characterized by the formation of a thick layer of base metal sulfide. Although Ni-20Si showed substantial degradation in some areas associated with preexisting cracks, this alloy was somewhat resistant as a result of the formation of a SiO_2 scale. It seemed that the only degradation of Ni-20Si was associated with alloy brittleness. This effect on sulfidation/oxidation was explained previously. Ni-20Si will provide adequate resistance to complex environments when superior alloy preparation techniques are employed.

CONCLUSIONS

Cr_2O_3 - Formers

The breakdown mechanisms of preformed Cr_2O_3 scales formed on M-Cr (M= Ni, Fe and Co) have been studied at 950°C at low oxygen and high sulfur potentials.

The relative growth rates of the scales in air are in the order of Fe-25Cr > Co-30Cr > Ni-30Cr. Those in sulfur-bearing gases are in the order of Ni-30Cr > Fe-25Cr > Co-30Cr.

For Cr_2O_3 on Ni-30Cr, degradation is initiated at the scale/alloy interface in sulfur-bearing gases. Sulfur penetration occurs through thin areas in the Cr_2O_3 scale. Voids that formed during preoxidation act as

barriers to chromium diffusion resulting in localized thinning of the Cr_2O_3 layer. Internal sulfides form at the rim of the voids where the chromium activity is high and grow to fill in the voids. Progressive formation of sulfides through the scale establish sulfide rich channels which are easy paths for cation transport. Scale breakdown occurs once the channels are introduced.

Breakdown of preformed oxide scales on Fe-25Cr is initiated at the scale/gas interface probably because of higher diffusivity of Fe through the oxide scale and impure oxide scale.

Degradation of preformed oxide scales on Co-30Cr is also initiated at the scale/gas interface probably due to the higher diffusivity of Co through the oxide scale.

Al_2O_3 - Formers

The breakdown mechanisms of preformed Al_2O_3 scales formed M-Cr-Al alloys with and without oxygen active elements have been studied at 950°C at low oxygen and high sulfur potentials.

For Fe-base alloys, the addition of Ti and Hf to Fe-18Cr-6Al improves the resistance to oxidation in air and to sulfidation/oxidation in sulfur-bearing gases at 950°C because of improved scale adherence. However, while Hf additions extend the life of FeCrAl alloys by improving adherence, they also provide phases in the scale which are vulnerable to sulfur penetration. Addition of Ti to FeCrAl, on the other hand, provides improved scale adherence without providing paths for sulfur ingress.

For Co-base alloys, the resistance to sulfidation/oxidation is fairly good and is comparable to that of Fe-18Cr-6Al-1Ti despite the formation of

external Cr_2O_3 scale after preoxidation. This is probably due to the higher dissociation pressure of cobalt sulfide compared to nickel and iron sulfide.

The resistance of the Ni-base alloys is worst among the alloys studied. The formation of a Cr_2O_3 layer during preoxidation and Ni-sulfides during exposure make this alloy ineffective in sulfur-bearing gases. With higher concentrations of Al (>6%), the protectiveness may be improved.

SiO_2 - Formers

The corrosion mechanism of SiO_2-forming alloys (Ni-20Si, Fe-20Si and Co-20Si) was studied between 700 and 950°C in oxidizing (air or H_2/H_2O) and sulfidizing (H_2/H_2S, $H_2/H_2S/H_2O$) atmospheres. Of particular interest was the breakdown of preformed oxide scales on Ni-20Si and Fe-20Si in $H_2/H_2O/H_2S$ atmospheres at the same temperatures and evaluation of stability of SiO_2-forming alloys upon exposure to syngas for a long period of time.

The overall resistance to isothermal oxidation in air and sulfidation/oxidation of Ni-20Si and Fe-20Si at 950°C was generally better than that of typical Cr_2O_3- and Al_2O_3-forming alloys.

Ni-20Si suffered vaporization losses in the sulfidizing atmosphere (H_2/H_2S) due to the high vapor pressure of SiS. However, vitreous silica scales formed on Ni-20Si were extremely resistant to sulfur penetration in the cyclic sulfidation/oxidation for a period of 44 hours. Even upon exposure to a severe environment (syngas), SiO_2 scales formed on Ni-20Si remained protective unless there were cracks in the starting material.

Fe-20Si was reistant to sulfur penetration initially despite the observation of small sulfide particles (FeS). In the cyclic sulfidation/oxidation experiment this alloy suffered a substantial amount of

degradation. Degradation was significant upon exposure to syngas and attack was characterized by the formation of a thick layer of base metal sulfide (FeS).

Co-20Si exhibited the worst sulfidation resistance among the alloys. The breakdown of SiO_2 films on Co-20Si was initiated at the scale/gas interface.

REFERENCES

1. K. Natesan, "High Temperature Corrosion in Coal Gasification Systems", Corrosion, Vol. 18, 1985, p. 646.

2. R. A. Perkins and S. J. Vonk, "Corrosion Chemistry in Low Oxygen Activity Atmospheres", Tech. report 979-6. Lockheed Palo Alto Research Laboratory, December 1979.

3. A. U. Seybolt, "Sulfur Diffusion Through Cr_2O_3 at 1000°C, AIME, Vol. 242, 1968, p. 752.

4. W. C. Hagel, "Anion Diffusion in Cr_2O_3," Journal of American Ceramic Society, Vol. 18, 1965, p.70.

5. C. S. Giggins and F. S. Pettit, "Corrosion of Metals and Alloys in Mixed Gas Environments at Elevated temperatures", Oxidation of Metals, Vol. 14, 1980, p. 363.

6. F. H. Stott, F. M. Chong and C. A. Stirling, "Preoxidation for Protection of High Temperature Alloys in Environments of High Sulfur and Low Oxygen Potentials Pertinent to Gasification Processes", High Temperature Corrosion in Energy Systems", M. F. Rothman, ed., AIME, 1985, p. 253.

7. C. A. Stirling, "The Influence of Performed Cr_2O_3 Scales on the High Temperature Corrosion of Alloys in Sulfur-Containing Gases, Ph.D. Dissertation, University of Manchester, Institute of Science and Technology, 1985.

8. G. Romeo, H. S. Spacil and W. J. Pasko, "The Transport of Chromium in Cr_2O_3 Scales in Sulfidizing Environments," Journal of Electrochemical Society, Vo. 122, 1975, p. 1329.

9. A. Rahmel, "Kinetic Conditions for the Simultaneous Formation of Oxide and Sulfide in Reaction of Iron with Gases Containing Sulfur and Oxygen or Their Compounds", Corrosion Science", Vol. 13, 1973, p. 125.

10. D. Bruce and P. Hancock, "Influence of Mechanical Properties of Surface Oxide Films on Oxidation Mechanism", Journal of Institute of Metals, Vol. 97, 1969, p. 140, 148.

11. T. T. Huang, B. Peterson, D. A. Shores and E. Pfender, "XPS and AES studies of High Temperature Corrosion Mechanism of Fe-30Cr Alloys", Corrosion Science, Vol. 24, 1984, p. 167.

12. T. T. Huang, R. Richter, Y. L. Chang and E. Pfender, "Formation of Aluminum Oxide Scales in Sulfur-Containing High Temperature Environments," Metallurgical Transaction A, Vol. 16A 1985, p. 2051.

13. R. A. Perkins, W. C. Coons and S. J. Vonk, "Materials Problems in Fluidized Bed Combustion and Coal Gasification Systems," Tech. report EPRI-CS-2452, Lockheed Palo Alto Research Laboratory, 1982.

14. F. H. Stott and M. F. Chong, "The Influence of Preoxidation on the Degradation of Alloys in Sulfur-Containing Gases at High Temperature", Corrosion resistant Materials for Coal Conversion Systems, D. B. Meadowcroft and M. I. Manning, ed., Applied Science Publishers, London and New York, 1983, p. 491.

15 P. A. Mari, J. M. Chaix and J. P. Larpin, "Protection of Fe-Cr-Al Alloys in Sulfidizing Environments by Means of Al_2O_3 Scale", Oxidation of Metals, Vol. 17, 1982, p. 315.

16. T. T. Huang, Y. C. Lin, D. A. Shores and E. Pfender, "Corrosion of FeCrAl, FeCrAlY and FeCrAlHf Alloys in High Temperature H_2-H_2S-H_2O Environment", Journal of Electrochemical Society, Vol. 131, 1984, p. 2191.

17. T. T. Huang, R. Richter and E. Pfender, "High Temperature Oxidation of Fe-18Cr-6Al Alloy in $H_2/H_2O/H_2S$ Gaseous Environments," High Temperature Corrosion in Energy Systems, M. F. Rothman, ed., AIME, 1985, p. 281.

18. A. W. Funkenbush, J. G. Smeggil and N. S. Bornstein, "Reactive Element-Sulfur Interaction and Oxide Scale Adherence," Metallurgical Transaction A, Vol. 16A, 1985, p. 1164.

19. Y. K. Kim, K. Pryzbylski, and G. J. Yurek, "in Proceedings of Symposium on Fundamental Aspects of High Temperature Corrosion, Vol. II," D. A. Shores and G. J. Yurek, ed., Electrochemical Society, 1986, p. 259.

20. T. Adachi and G. H. Meier, "Oxidation of Iron-Silicon Alloys," Oxidation of Metals, Vol. 27,5/6 1987, p. 347.

21. D. L. Douglas, P. Nanni, C. De Asmundis, and C. Bottino, "The Transition from Internal Oxidation to Continuous-Film Formation during Oxidation of Dilute Ni-Si Alloy," Oxidation of Metals, Vol. 28,5/6 1987, p. 309.

22. F. H. Stott, G. J. Gabriel, and G. C. Wood, "The Influence of Silicon on the High-Temperature Oxidation of Nickel", Oxidation of Metals, Vol. 28,5/6 1987, p. 329.

23. G. M. Kim, E. A. Gulbransen and G. H. Meier, "Corrosion of SiO_2 Forming Alloys in Sulfidizing/Oxidizing Atmospheres," in Performance of High Temperature Materials in Fluidized Bed Compbustion Systems and Process Industries, P. Ganesan and R. A. Bradley, ed., ASM International, 1987, p. 129.

24. E. A. Gulbransen and K. F. Andrew, "Vapor Pressure studies on Iron and Chromium and Several Alloys of Iron, Chromium and Aluminum", Transactions of the Metallurgical Society of AIME", Vol. 221, 1961, p. 1247.

25. O. Kubaschewski and G. Heyer, "The Thermodynamics of the Chromium-Iron System", Acta Metallurgica, Vol. 8, 1960, p. 416.

26. T. Azhar, "Thermodynamic and Kinetic Analysis of Ni-Cr-O-S,Ni-Al-O-S and Ni-Si-O-S Systems", Masters Thesis, University of Pittsburgh", 1986.

27. N. Birks and G. H. Meier, "Introduction to High Temperature Oxidation of Metals", Edward Arnold, London, 1983.

28. S. Mrowec and K. Przybylski, "Transport Properties of Sulfide Scales and Sulfidation of Metals and Alloys", Oxidation of Metals, Vol. 23, 1985, p. 107.

29. E. J. Vinverg and D. L. Douglass, "The Sulfidation Behavior of Nickel-Chromium and Nickel-Aluminum bearing Alloys with and without Yttrium", High Temperature Corrosion Transactions, Japan Institute of Metals, 1983, p. 507.

30. G. M. Kim and G. H. Meier, "Breakdown of Preformed Oxides on Ni- and Fe-Base Alloys in High Sulfur Pressure Atmospheres," in High Temperature Materials Chemistry - IV, Z. A. Munir, D. Cubicciotti, and H. Tagawa eds., The Electrochemical Soc., 1988, p. 79.

31. G. M. Kim, The Breakdown of Preformed Oxide Scales on Ni-30Cr, Fe-18Cr-6Al-1Hf and Ni-20Si in Sulfur and Carbon-Bearing Gases, Ph.D. dissertation, University of Pittsburgh,1986.

32. G. J. Yurek and M. H. LaBranche, "Oxidation of Chromium in $H_2/H_2O/H_2S$ Gas Mixture", Corrosion-Erosion-Wear of Materials in Emerging Fossil Energy Systems, A. V. Levy, ed., NACE, Berkeley, California, 1982, p. 933

33. T. B. Massalski, J. L. Murray, L. H. Bennett and H. Baker, Binary Alloy Phase Diagrams, American Society for Metals, 1980.

Figure 1: Stability Diagrams for the M (Cr, Si, Al, Hf, Ti, Fe, Ni and Co)-S-O systems at 950°C. Representative gas compositions are illustrated.

Figure 2: Weight changes vs. time for Fe-25Cr, Co-30Cr and Ni-30Cr during oxidation in air at 950°C.

Figure 3: Ni-30Cr exposed to a H_2/H_2O gas mixture for 30 minutes and subsequently exposed to a $H_2/H_2O/H_2S$ gas mixture for 5 minutes at 950°C.

Figure 4: Ni-30Cr exposed to a H_2/H_2O gas mixture for 30 minutes and subsequently exposed to a $H_2/H_2O/H_2S$ gas for 10 minutes at 950°C. (a) external oxide scale (b) underside of oxide scale and (c) alloy substrate.

Figure 5: Ni-30Cr exposed to a H_2/H_2O gas mixture for 30 minutes and subsequently exposed to a $H_2/H_2O/H_2S$ gas for 20 minutes at 950°C. (a) external oxide scale (b) underside of oxide scale and (c) alloy substrate.

Figure 6: Taper polished specimen of Ni-30Cr which was exposed to a H_2/H_2O mixture for 30 minutes and subsequently exposed to $H_2/H_2O/H_2S$ gas mixture for 10 minutes. (a) taper polished external scale and (b) underside of the oxide scale.

Figure 7: Morphologies of the external scale surface and the alloy substrate of Ni-30Cr after 30 minutes of oxidation in a H_2/H_2O gas composition at 950°C.

Figure 8: Schematic drawing of different oxide thickness due to the formation of a void at the scale/alloy interface.

Figure 9: Concentration profile of sulfur on Ni-30Cr which was oxidized in a H_2/H_2O gas mixture for 30 minutes and subsequently exposed to a $H_2/H_2O/H_2S$ gas mixture for 4 hours at 700°C.

Figure 10: Schematic representation of the breakdown of preformed Cr_2O_3 scale formed on Ni-30Cr by sulfur-bearing gases.

Figure 11: Fe-25Cr exposed to a H_2/H_2O gas mixture for 5 hours and subsequently exposed to a $H_2/H_2O/H_2S$ gas mixture for 10 minutes at 950°C. (a) external oxide scale (b) underside of the scale.

Figure 12: Fe-25Cr exposed to a H_2/H_2O gas mixture for 5 hours and subsequently exposed to a $H_2/H_2O/H_2S$ gas mixture at 950°C. (a) 10 minutes, (b) 20 minutes, (c) 1 hour and (d) 2 hours.

Figure 13: Fe-25Cr exposed to a H_2/H_2O gas mixture for 5 hours at 950°C. (a) the scale/gas interface, (b) the scale/alloy interface and (c) cross section.

Figure 14: Co-30Cr exposed to a H_2/H_2O gas mixture for 5 hours and subsequently exposed to a $H_2/H_2O/H_2S$ gas mixture at 950°C. (a) 10 minutes and (b) 20 minutes.

Figure 15: Weight changes vs. time for the alloys during oxidation in air at 950°C.

Figure 16: Surface morphologies of Fe-18Cr-6Al-1Hf exposed to a H_2/H_2O gas mixture for 30 minutes and subsequently exposed to a $H_2/H_2S/H_2O$ gas mixture for 4 hours.

Figure 17: Fe-18Cr-6Al-1Hf exposed to a H_2/H_2O gas mixture for 30 minutes and subsequently exposed to a $H_2/H_2S/H_2O$ gas mixture for 4 hours at 950°C. (a) external oxide scale (b) underside of the scale and (c) alloy substrate.

Figure 18: Morphologies of (a) the external scale surface, (b) the underside of scale and (c) the alloy substrate of Fe-18Cr-6Al-1Hf after 30 minutes of oxidation at 950°C in a H_2/H_2O gas composition

Figure 19: Fe-18Cr-6Al-1Hf exposed to a H_2/H_2O gas mixture for 30 minutes and subsequently exposed to a $H_2/H_2O/H_2S$ gas mixture for 4 hours at 950°C. (a) external sulfide morphology and (b) transverse section.

Figure 20: Fe-18Cr-6Al-1Hf exposed to a H_2/H_2O gas mixture for 30 minutes and subsequently exposed to a $H_2/H_2S/H_2O$ gas mixture for 4 hours at 950°C.

Figure 21: Fe-18Cr-6Al exposed to a H_2/H_2O gas mixture for 30 minutes and subsequently exposed to a $H_2/H_2S/H_2O$ gas mixture for 4 hours at 950°C. (a) after preoxidation and (b) after sulfidation-oxidation.

Figure 22: Schematic representation of the breakdown of preformed Al_2O_3 scale formed on (a) Fe-18Cr-6Al and (b) Fe-18Cr-6Al-1Hf by sulfur-bearing gases.

Figure 23: Weight changes vs time for cyclic oxidation of Fe-18Cr-6Al, Fe-18Cr-6Al-1Hf, and Fe-18Cr-6Al-1Ti in air at 1100°C.

Figure 24: Weight changes vs time for Fe-18Cr-6Al-1Ti and Fe-18Cr-6Al-1Hf which were preoxidized in a H_2/H_2O mixture and subsequently exposed to a $H_2/H_2O/H_2S$ mixture at 950°C.

Figure 25: Co-18Cr-6Al-1Hf exposed to a H_2/H_2O gas mixture for 2 hours and subsequently exposed to a $H_2/H_2S/H_2O$ gas mixture for 4 hours at 950°C.

Figure 26: Ni-18Cr-6Al-1Hf exposed to a H_2/H_2O gas mixture for 2 hours and subsequently exposed to a $H_2/H_2S/H_2O$ gas mixture for 4 hours at 950°C.

Figure 27: Weight changes vs. time for cyclic sulfidation/oxidation (4 hour cycles) in a $H_2/H_2S/H_2O$ gas mixture after preoxidation in a H_2/H_2O gas mixture for 30 minutes at 950°C.

Figure 28: Cross-sections of (a) Fe-Cr-Al-Ti, (b) Fe-Cr-Al-Hf, and (c) Co-Cr-Al-Hf after 995 hrs. exposure in a syngas atmosphere at 550°c.

Figure 29: Weight changes vs. time for the alloys during oxidation in air at 950°C.

Figure 30: TEM micrograph of Ni-20Si oxidized in air at 950°C for an hour with selected area diffraction patterns.

Figure 31: Silica forming alloys sulfidized in a H_2/H_2S gas mixture at 950°C for 4 hours. (a) Ni-20Si (b) Fe-20Si and (C) Co-20Si.

Figure 32: Vapor species diagram for the Si-S system at 950°C.

Figure 33: Schematic representation of degradation of Ni-20Si in a H_2/H_2S gas mixture at 950°C.

Figure 34: Ni-20Si exposed to a H_2/H_2O gas mixture for 30 minutes and subsequently exposed to a $H_2/H_2O/H_2S$ gas mixture for 4 hours at 950°C.

Figure 35: Ni-20Si exposed to a H_2/H_2O gas mixture for 30 minutes and subsequently exposed to a $H_2/H_2O/H_2S$ gas mixture for 4 hours at 950°C.

Figure 36: Schematic representation of the breakdown of preformed SiO_2 scale formed on Ni-20Si by sulfur-bearing gases.

Figure 37: Fe-20Si exposed to a H_2/H_2O gas mixture or 30 minutes and subsequently exposed to a $H_2/H_2O/H_2S$ gas mixture for 4 hours at 700°C. (a) external oxide scale (b) underside of the oxide scale.

Figure 38: Co-20Si exposed to a H_2/H_2O gas mixture for 30 minutes and subsequently exposed to a $H_2/H_2O/H_2S$ gas mixture for 4 hours at 950°C. (a) external oxide scale, (b) cross section of (a), and (c) EDX spectra of sulfide(arrow).

Figure 39: Weight changes vs. time for cyclic sulfidation/oxidation (4 hour cycles) in a $H_2/H_2S/H_2O$ gas mixture after preoxidation in a H_2/H_2O gas mixture for 30 minutes at 950°C.

Figure 40: Transverse sections of specimens after 44 hours of cyclic sulfidation/oxidation (4 hour cycle) in a $H_2/H_2S/H_2O$ gas mixture after preoxidation in a H_2/H_2O gas mixture for 30 minutes at 950°C. (a) Ni-20Si, (b) Fe-20Si and (c) Co-20Si.

Figure 41: Ni-20Si which was coated with gasifier slag and then exposed to syngas at 550°C for 160 hours. These show two different degradation areas. (a) Severely degraded area and (b) protective area.

Figure 42: Fe-20Si which was coated with gasifier slag and then exposed to syngas at 550°C for 160 hours.

TABLE 1. Nominal Alloy Compositions Expressed In Weight Percent

Chromia-Formers	Alumina-Formers	Silica-Formers
Ni-30Cr	Ni-18Cr-6Al-1Hf	Ni-20Si
Co-30Cr	Co-18Cr-6Al-1Hf	Co-20Si
Fe-25Cr	Fe-18Cr-6Al	Fe-20Si
	Fe-18Cr-6Al-1Hf	
	Fe-18Cr-6Al-1Ti	

TABLE 2. Weight changes after 4 hours of sulfidation-oxidation at 950°C.

Alloys	$H_2/H_2S/H_2O$ (log P_{S_2} = -6.1,	log P_{O_2} = -18.7)
		30 Min. Preox.
Ni-30Cr	55.74	20.20
Fe-25Cr	55.8	8.20
Co-30Cr	20.87	4.13

TABLE 3. Weight changes after 4 hours of sulfidation - Oxidation at 950°C.

	log PS2= -6.10	log PO2= -18.71 950°C 30 min	log PO2= -15.30 1150°C 30 min	log PO2= -18.71		log PS2= -6.10
					preox 950°C. 30 min.	preox 1150°C. 30 min
Ni-Cr	114.30	0.10	0.64	55.74	20.20	1.09
Fe-Cr-Al-Hf	23.25	negligible	0.11	5.90	0.35	0.48
Ni-Si	-4.53	-0.04	0.03	0.10	0.04	0.04

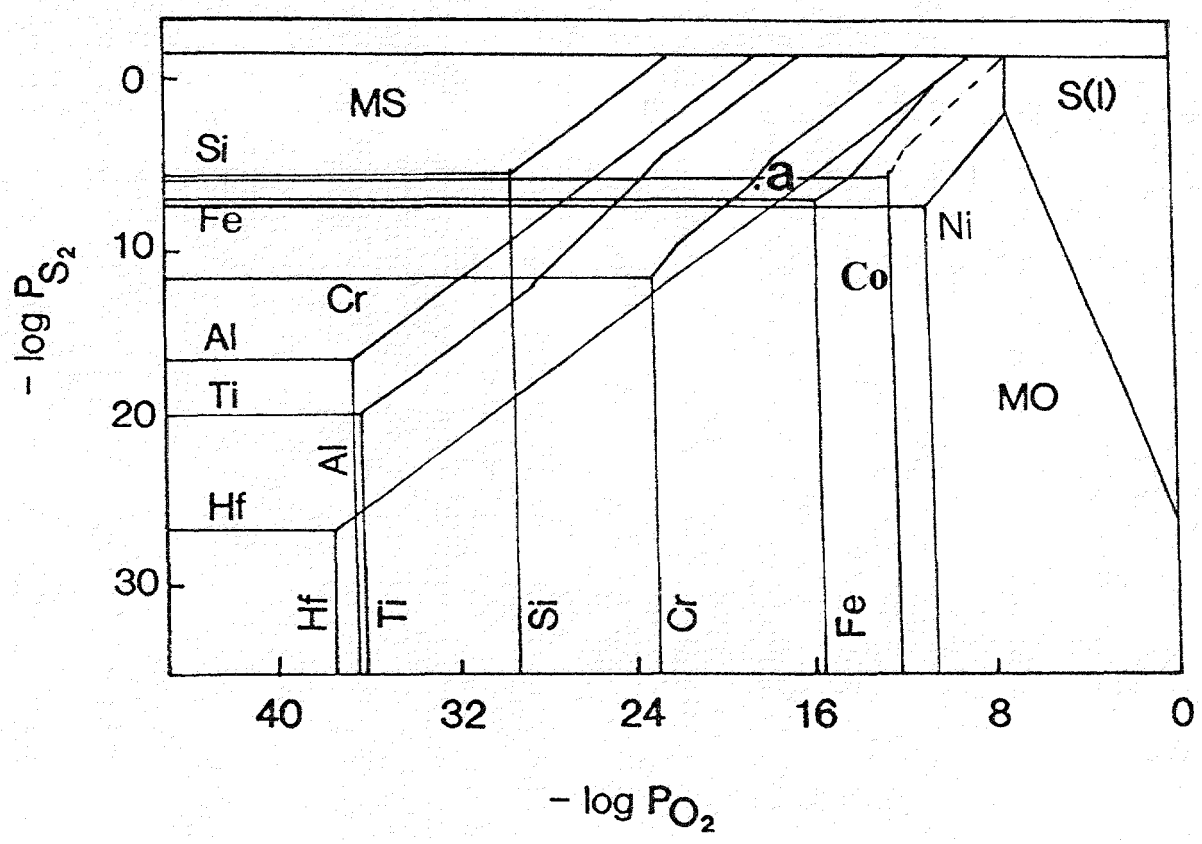

Figure 1: Stability Diagrams for the M (Cr, Si, Al, Hf, Ti, Fe, Ni and Co)-S-O systems at 950°C. Representative gas compositions are illustrated.

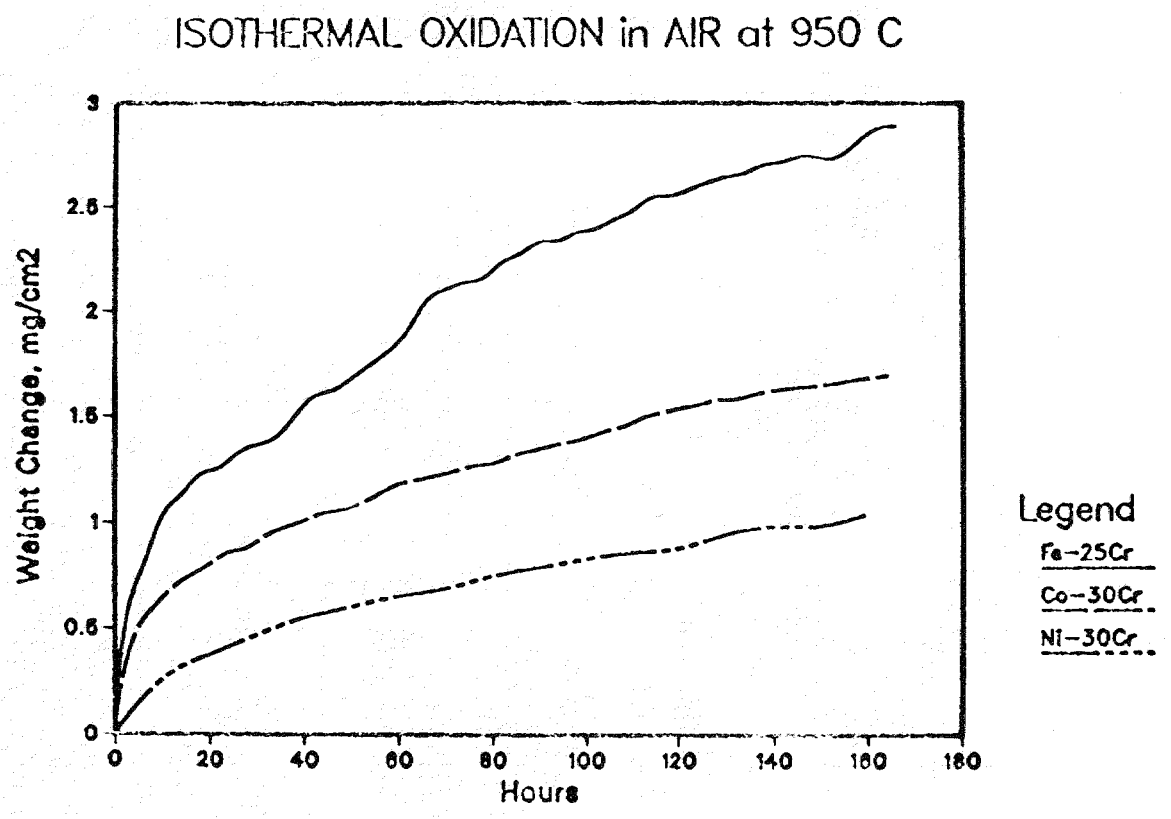

Figure 2: Weight changes vs. time for Fe-25Cr, Co-30Cr and Ni-30Cr during oxidation in air at 950°C.

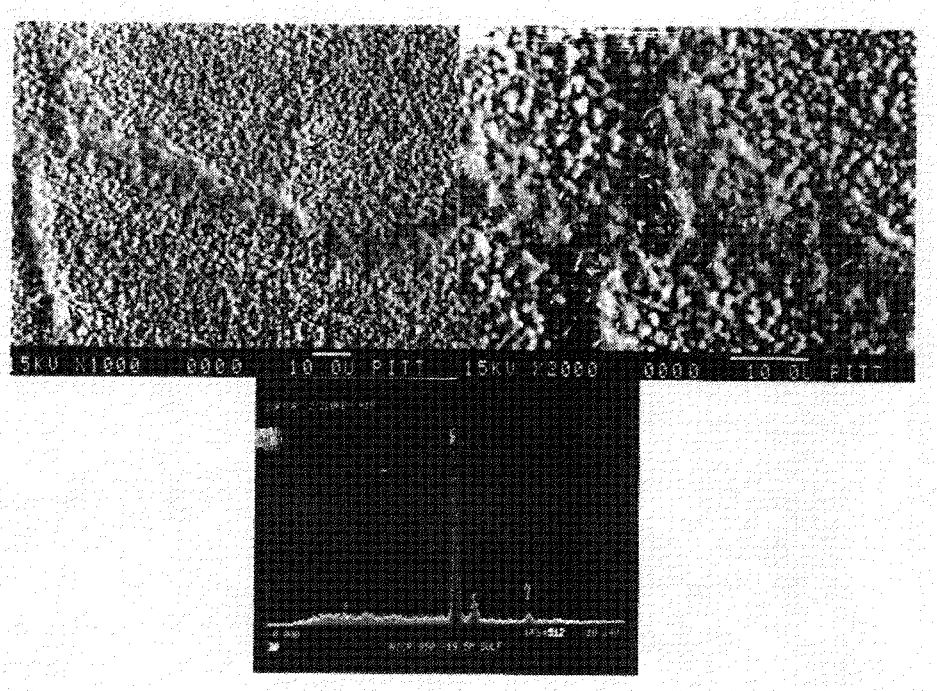

Figure 3: Ni-30Cr exposed to a H_2/H_2O gas mixture for 30 minutes and subsequently exposed to a $H_2/H_2O/H_2S$ gas mixture for 5 minutes at 950°C.

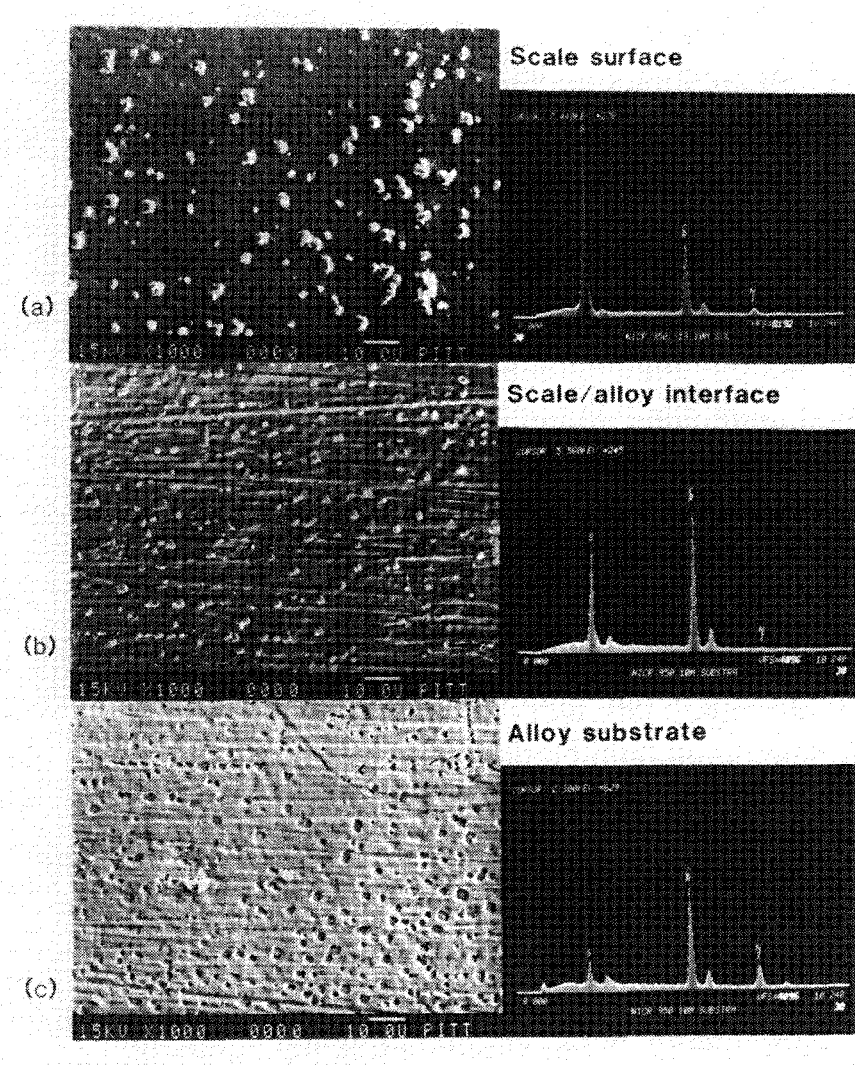

Figure 4: Ni-30Cr exposed to a H_2/H_2O gas mixture for 30 minutes and subsequently exposed to a $H_2/H_2O/H_2S$ gas for 10 minutes at 950°C. (a) external oxide scale (b) underside of oxide scale and (c) alloy substrate.

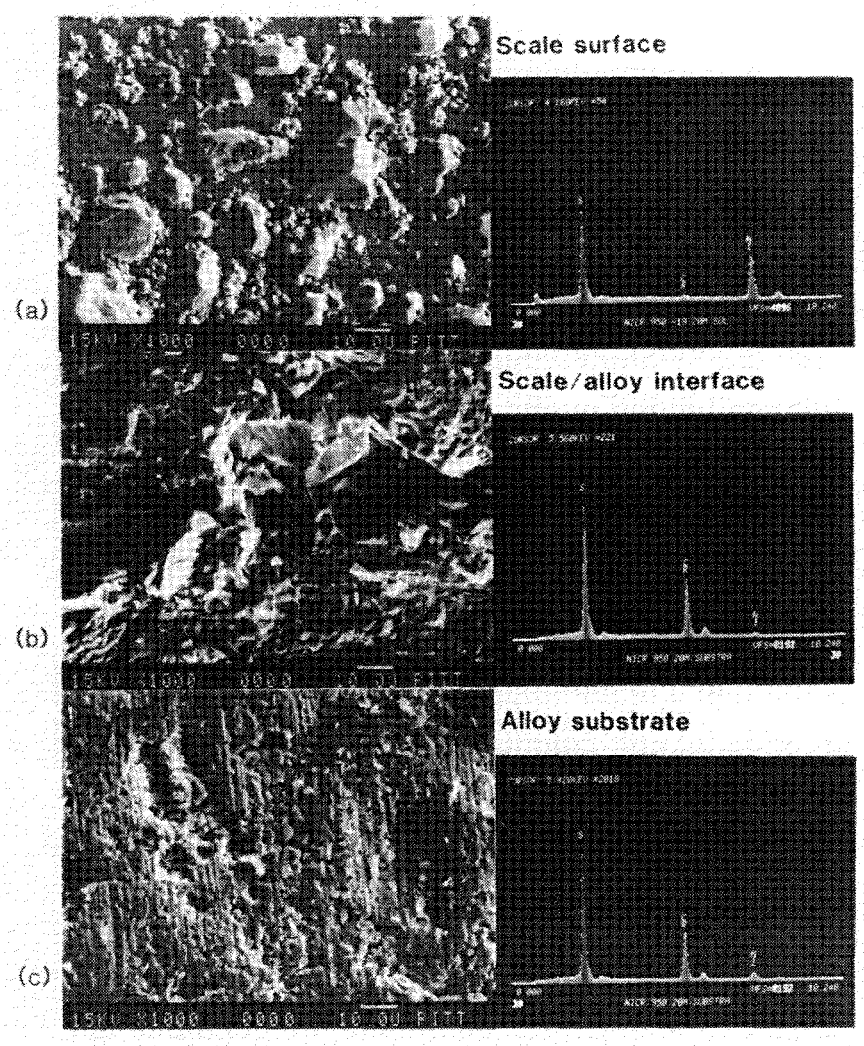

Figure 5: Ni-30Cr exposed to a H_2/H_2O gas mixture for 30 minutes and subsequently exposed to a $H_2/H_2O/H_2S$ gas for 20 minutes at 950°C. (a) external oxide scale (b) underside of oxide scale and (c) alloy substrate.

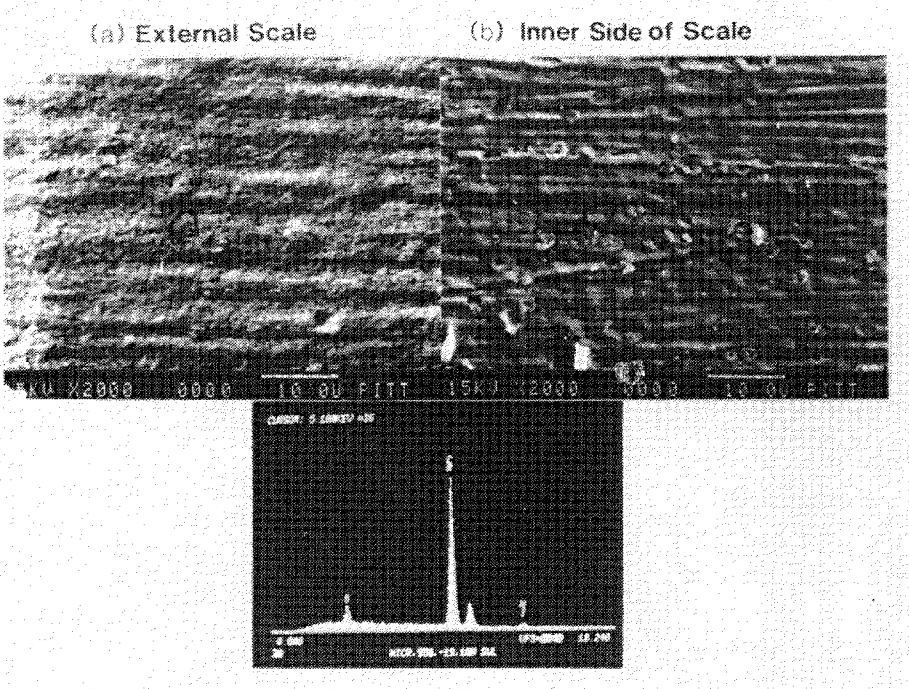

Figure 6: Taper polished specimen of Ni-30Cr which was exposed to a H_2/H_2O mixture for 30 minutes and subsequently exposed to $H_2/H_2O/H_2S$ gas mixture for 10 minutes. (a) taper polished external scale and (b) underside of the oxide scale.

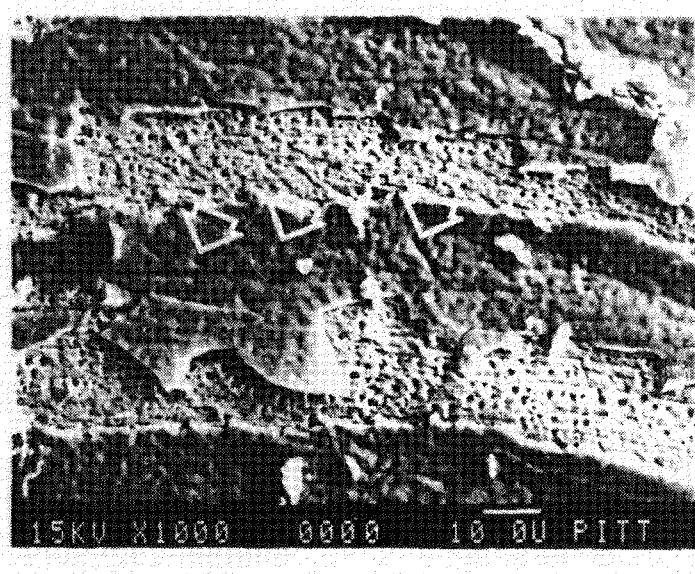

Figure 7: Morphologies of the external scale surface and the alloy substrate of Ni-30Cr after 30 minutes of oxidation in a H_2/H_2O gas composition at 950°C.

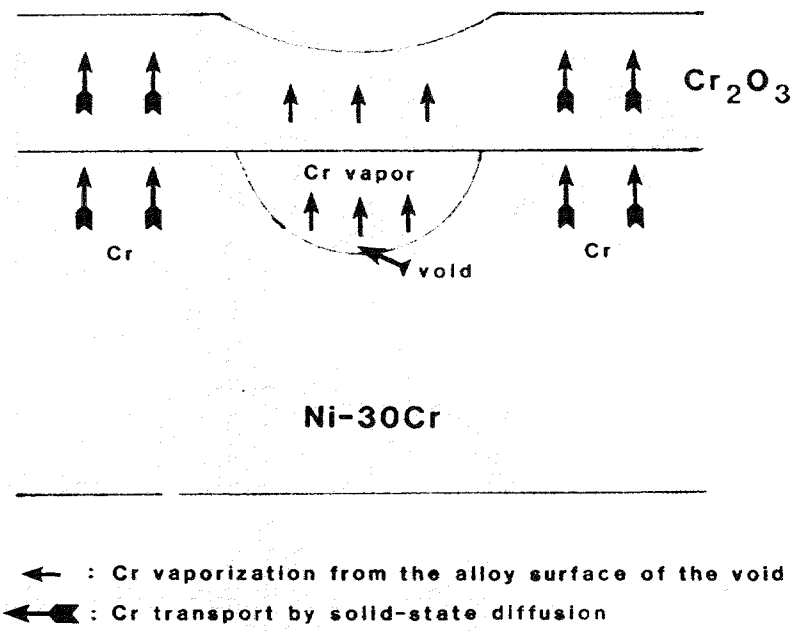

Figure 8: Schematic drawing of different oxide thickness due to the formation of a void at the scale/alloy interface.

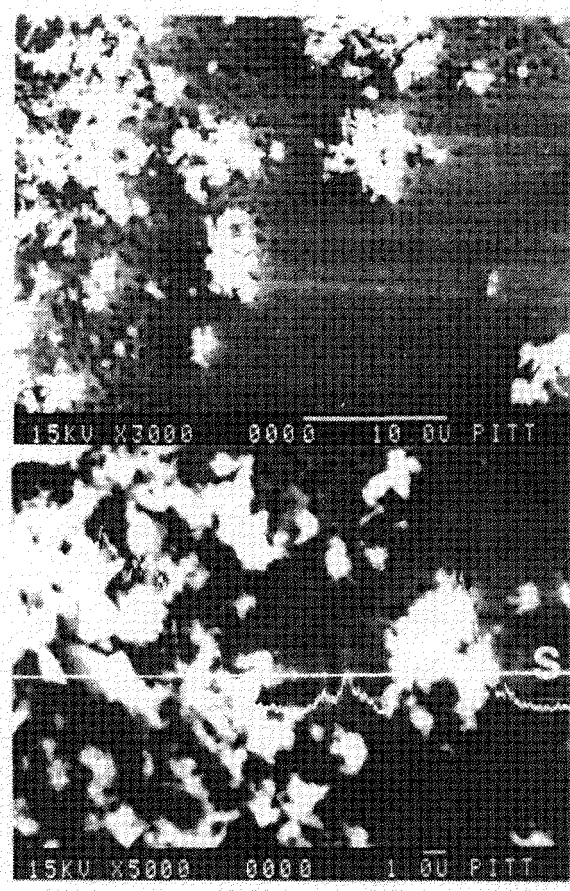

(a)

(b)

Figure 9: Concentration profile of sulfur on Ni-30Cr which was oxidized in a H_2/H_2O gas mixture for 30 minutes and subsequently exposed to a $H_2/H_2O/H_2S$ gas mixture for 4 hours at 700°C.

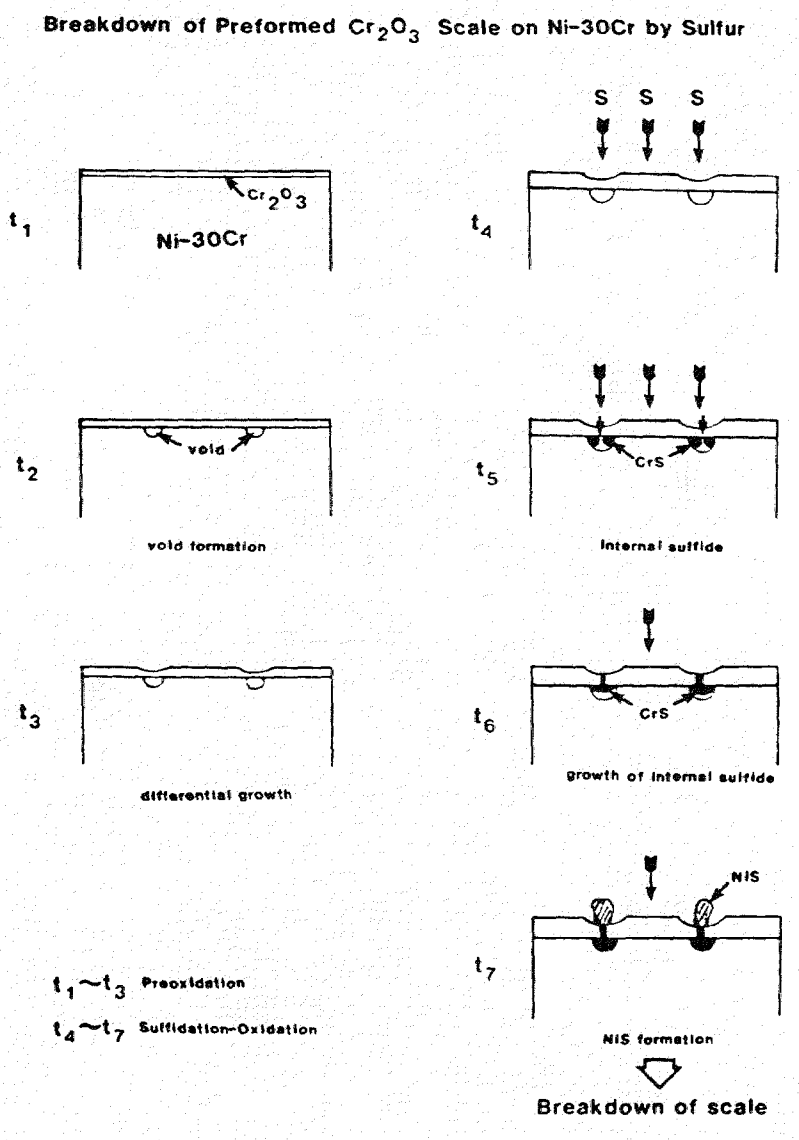

Figure 10: Schematic representation of the breakdown of preformed Cr_2O_3 scale formed on Ni-30Cr by sulfur-bearing gases.

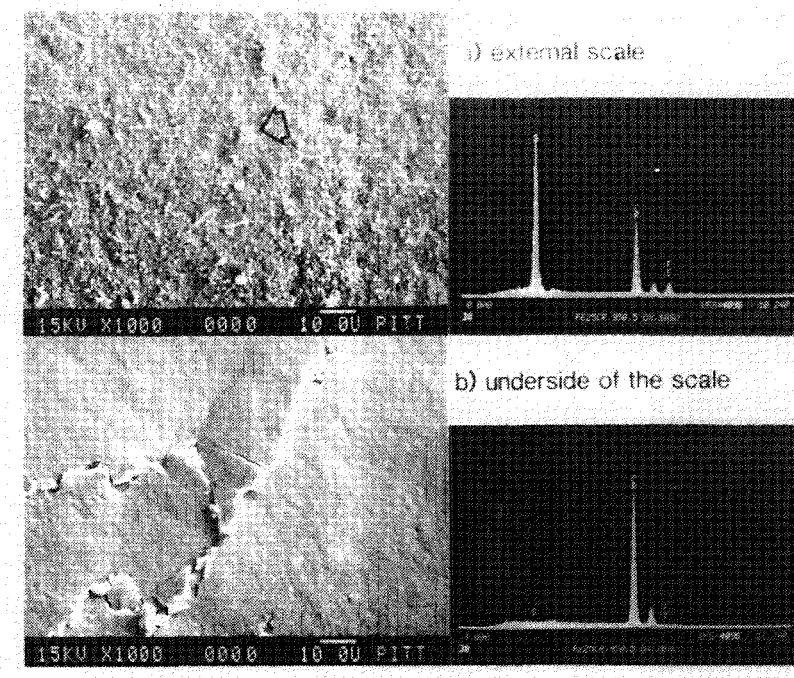

Figure 11: Fe-25Cr exposed to a H_2/H_2O gas mixture for 5 hours and subsequently exposed to a $H_2/H_2O/H_2S$ gas mixture for 10 minutes at 950°C. (a) external oxide scale (b) underside of the scale.

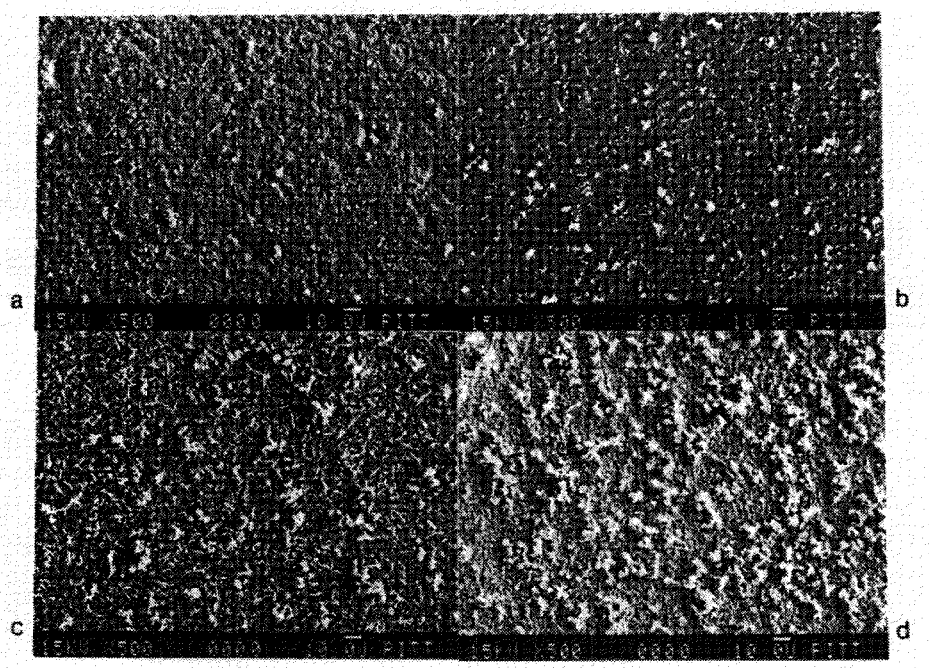

Figure 12: Fe-25Cr exposed to a H_2/H_2O gas mixture for 5 hours and subsequently exposed to a $H_2/H_2O/H_2S$ gas mixture at 950°C. (a) 10 minutes, (b) 20 minutes, (c) 1 hour and (d) 2 hours.

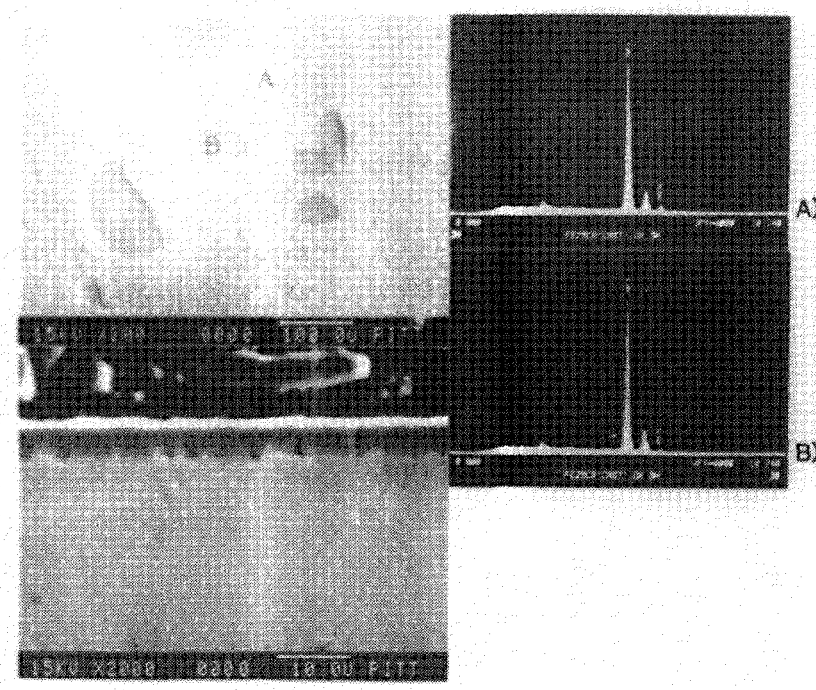

Figure 13: Fe-25Cr exposed to a H_2/H_2O gas mixture for 5 hours at 950°C. (a) the scale/gas interface, (b) the scale/alloy interface and (c) cross section.

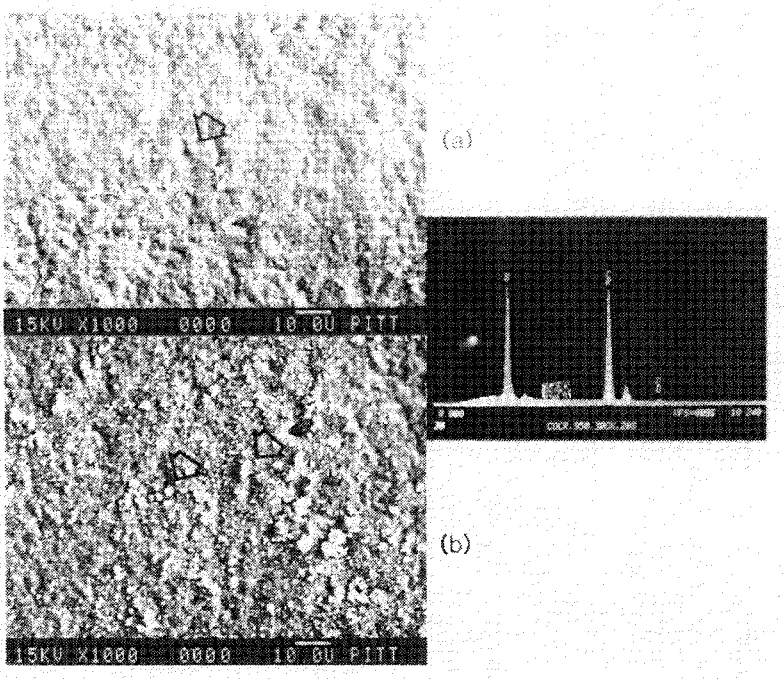

Figure 14: Co-30Cr exposed to a H_2/H_2O gas mixture for 5 hours and subsequently exposed to a $H_2/H_2O/H_2S$ gas mixture at 950°C. (a) 10 minutes and (b) 20 minutes.

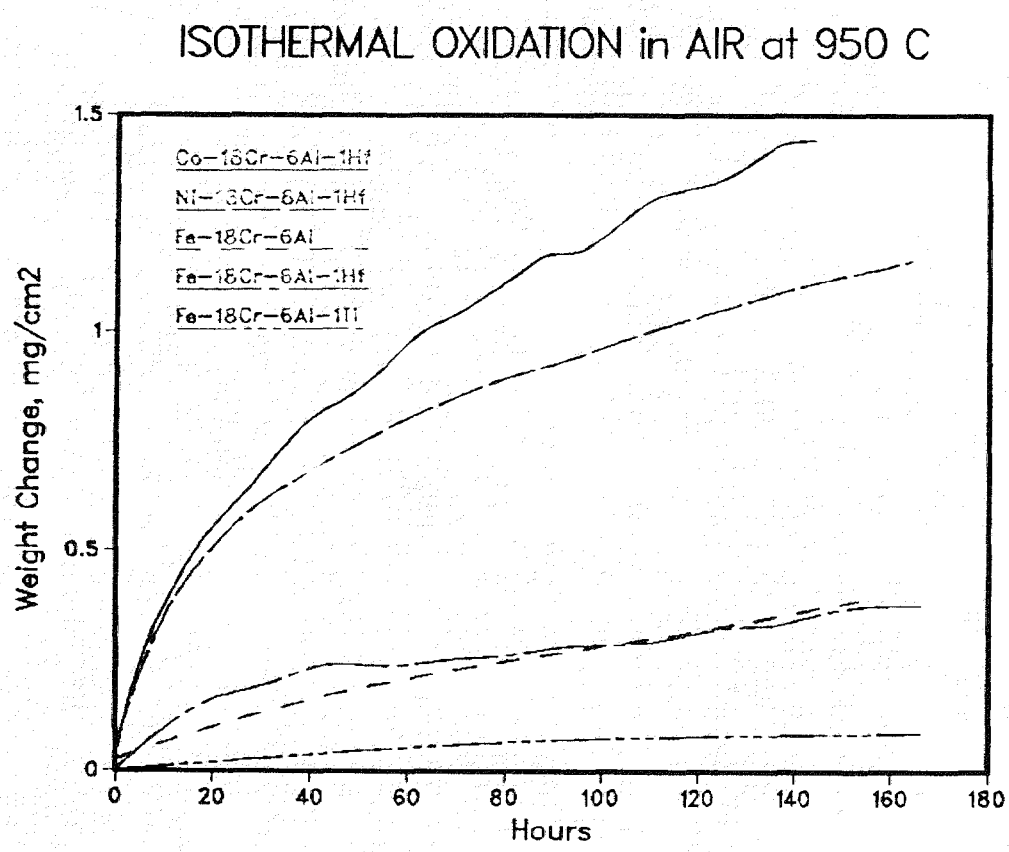

Figure 15: Weight changes vs. time for the alloys during oxidation in air at 950°C.

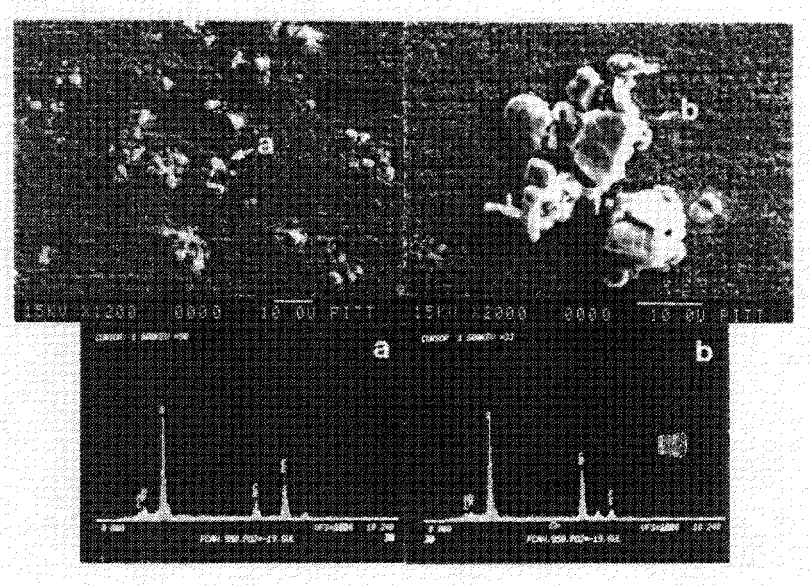

Figure 16: Surface morphologies of Fe-18Cr-6Al-1Hf exposed to a H_2/H_2O gas mixture for 30 minutes and subsequently exposed to a $H_2/H_2S/H_2O$ gas mixture for 4 hours.

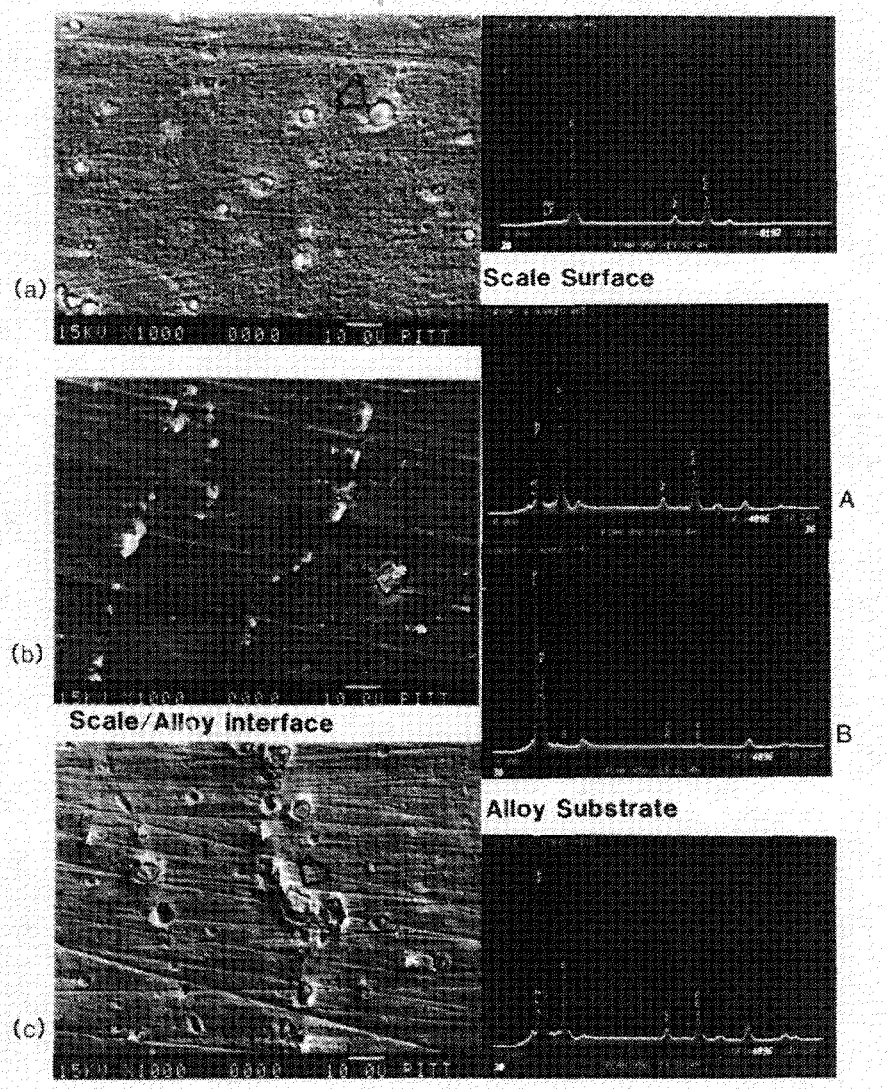

Figure 17: Fe-18Cr-6Al-1Hf exposed to a H_2/H_2O gas mixture for 30 minutes and subsequently exposed to a $H_2/H_2S/H_2O$ gas mixture for 4 hours at 950°C. (a) external oxide scale (b) underside of the scale and (c) alloy substrate.

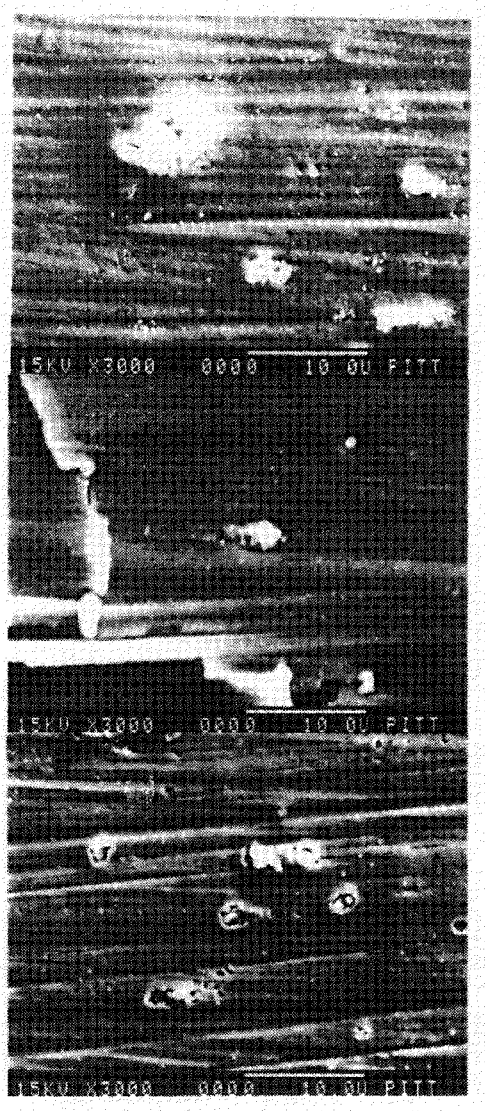

Figure 18: Morphologies of (a) the external scale surface, (b) the underside of scale and (c) the alloy substrate of Fe-18Cr-6Al-1Hf after 30 minutes of oxidation at 950°C in a H_2/H_2O gas composition

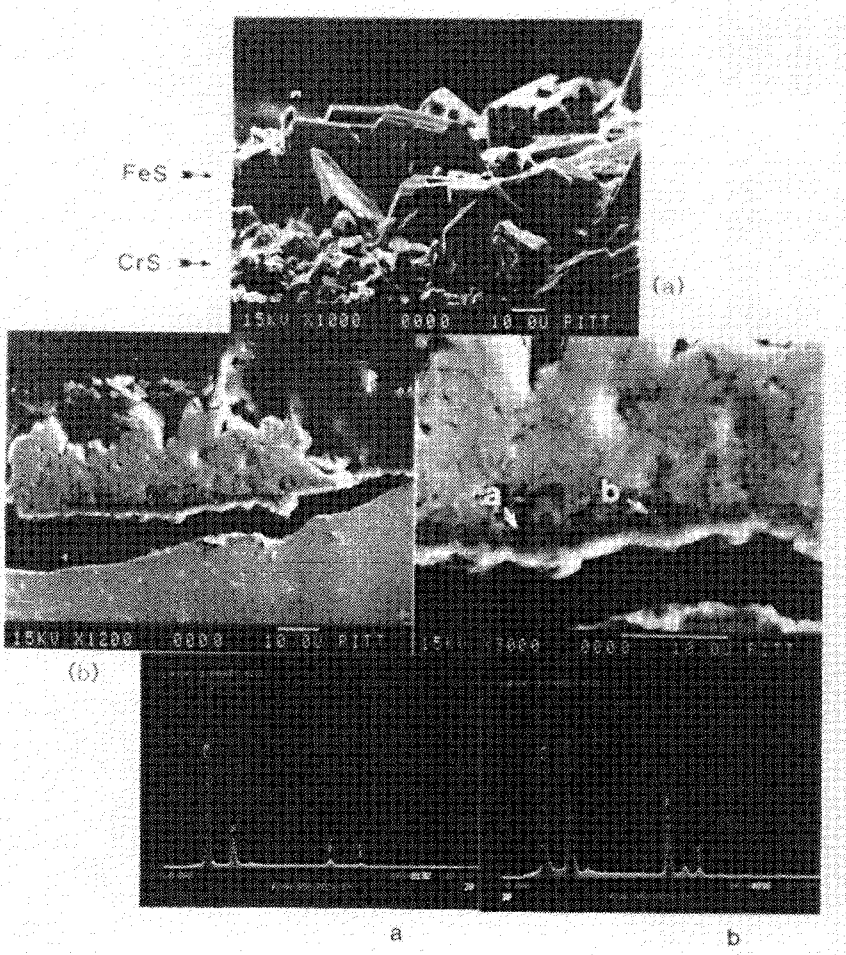

Figure 19: Fe-18Cr-6Al-1Hf exposed to a H_2/H_2O gas mixture for 30 minutes and subsequently exposed to a $H_2/H_2O/H_2S$ gas mixture for 4 hours at 950°C. (a) external sulfide morphology and (b) transverse section.

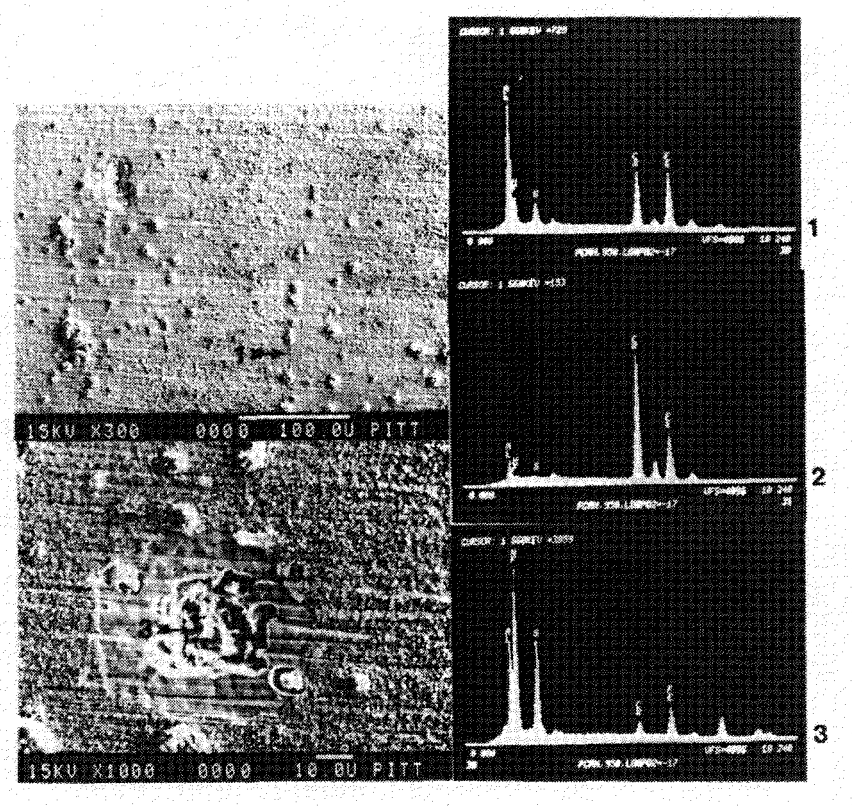

Figure 20: Fe-18Cr-6Al-1Hf exposed to a H_2/H_2O gas mixture for 30 minutes and subsequently exposed to a $H_2/H_2S/H_2O$ gas mixture for 4 hours at 950°C.

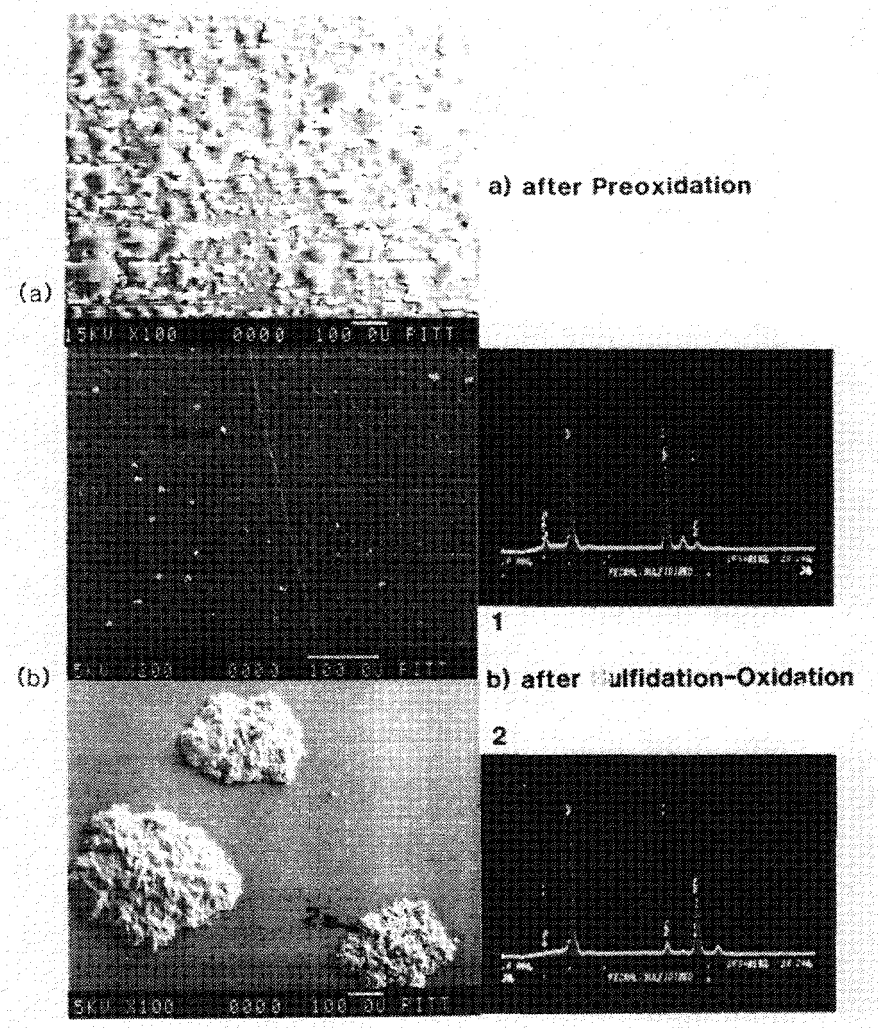

Figure 21: Fe-18Cr-6Al exposed to a H_2/H_2O gas mixture for 30 minutes and subsequently exposed to a $H_2/H_2S/H_2O$ gas mixture for 4 hours at 950°C. (a) after preoxidation and (b) after sulfidation-oxidation.

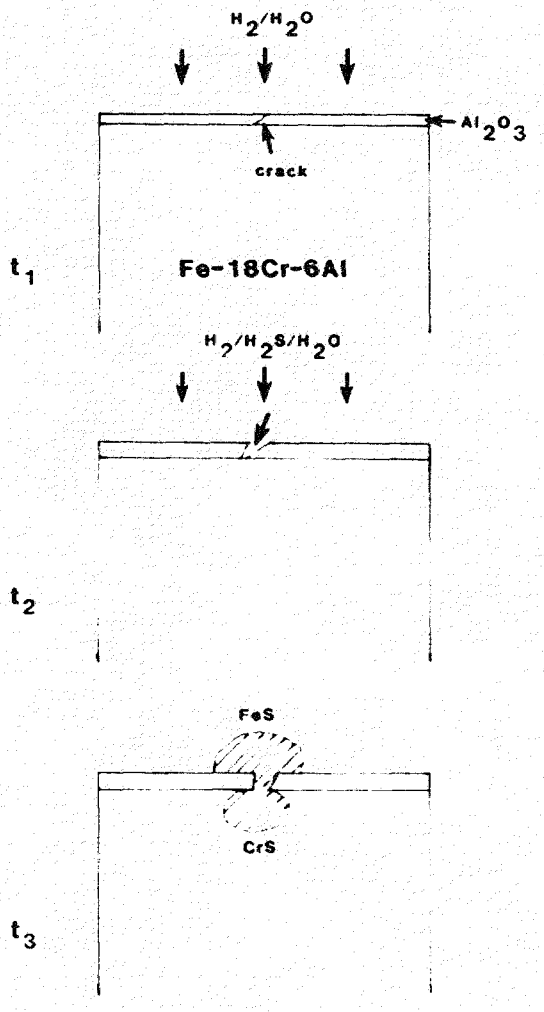

Figure 22: Schematic representation of the breakdown of preformed Al_2O_3 scale formed on (a) Fe-18Cr-6Al and (b) Fe-18Cr-6Al-1Hf by sulfur-bearing gases.

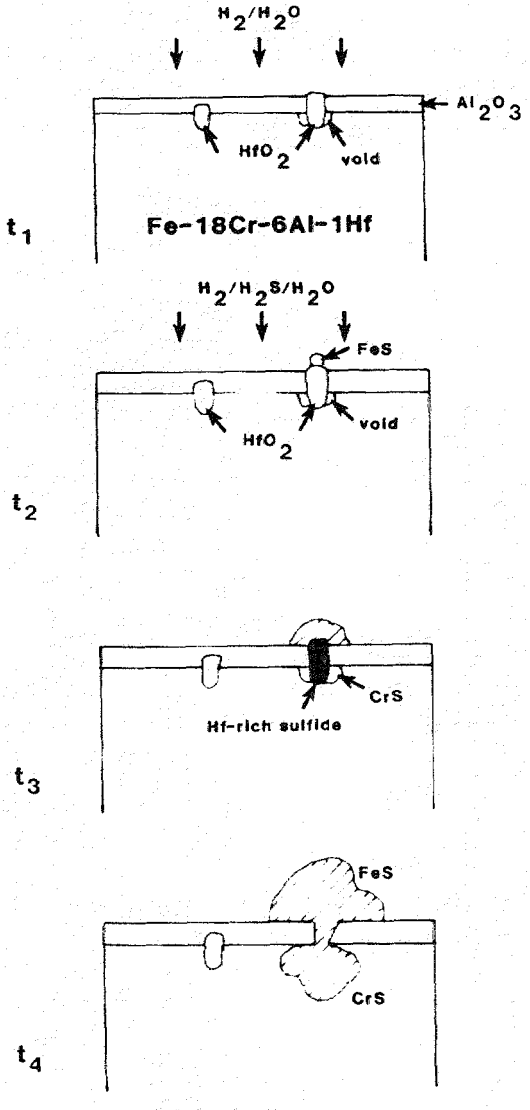

Figure 22: (Continued) Schematic representation of the breakdown of preformed Al_2O_3 scale formed on (a) Fe-18Cr-6Al and (b) Fe-18Cr-6Al-1Hf by sulfur-bearing gases.

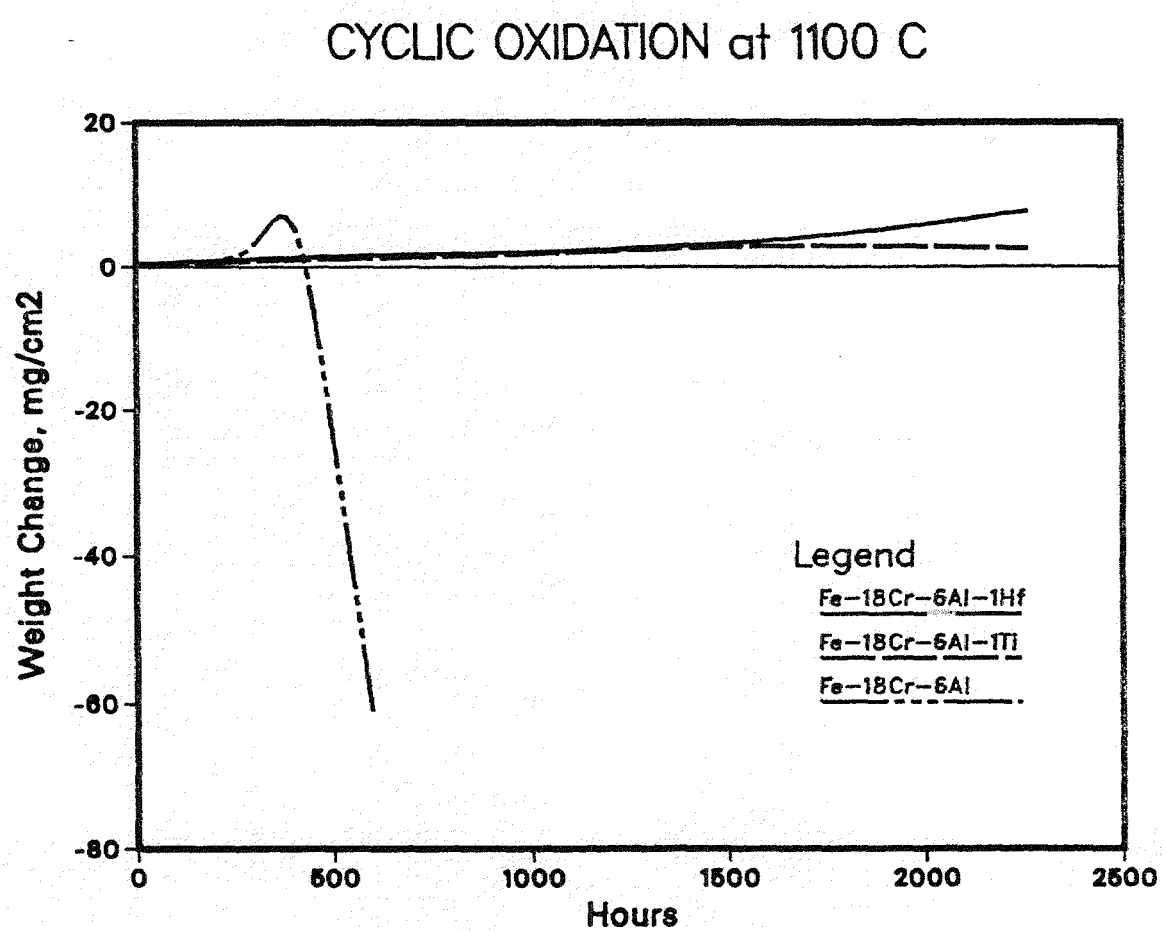

Figure 23: Weight changes vs time for cyclic oxidation of Fe-18Cr-6Al, Fe-18Cr-6Al-1Hf, and Fe-18Cr-6Al-1Ti in air at 1100°C.

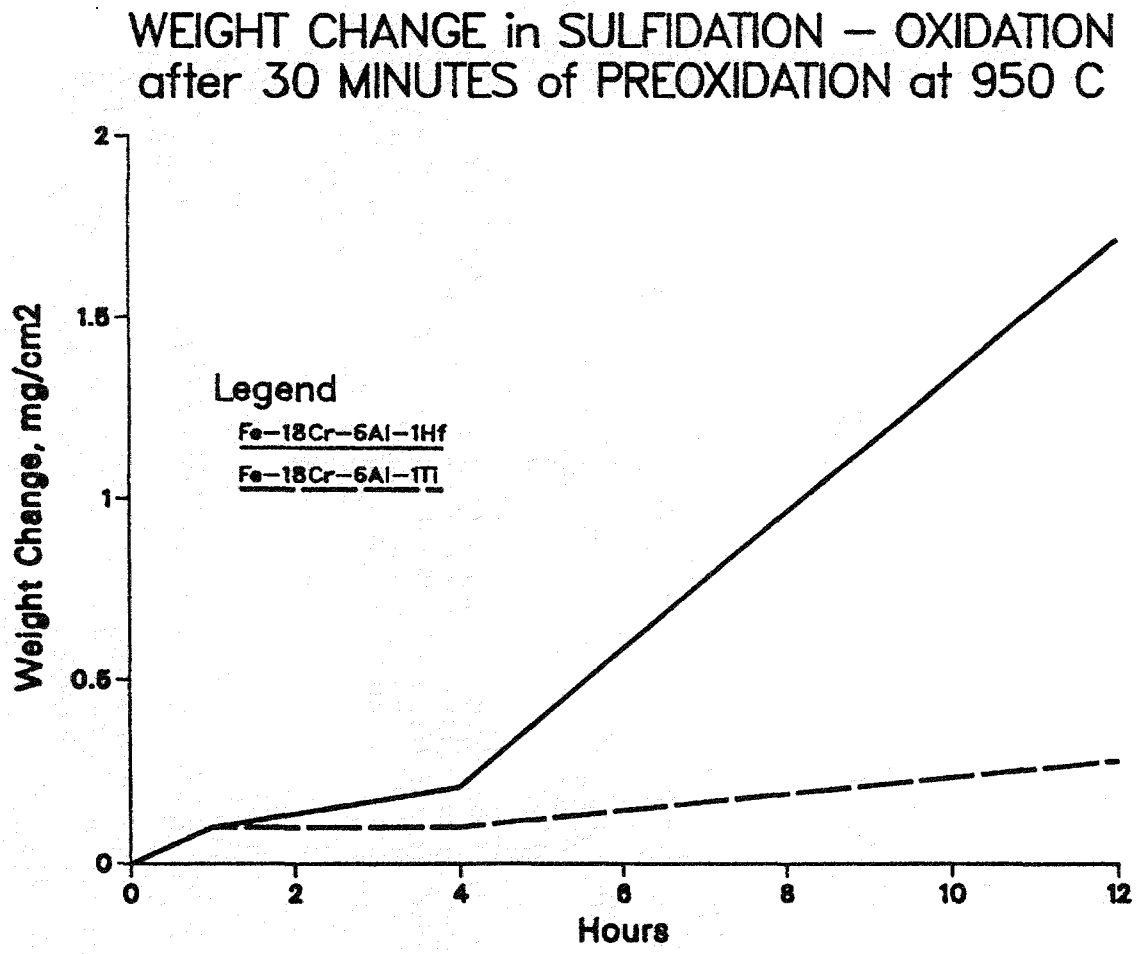

Figure 24: Weight changes vs time for Fe-18Cr-6Al-1Ti and Fe-18Cr-6Al-1Hf which were preoxidized in a H_2/H_2O mixture and subsequently exposed to a $H_2/H_2O/H_2S$ mixture at 950°C.

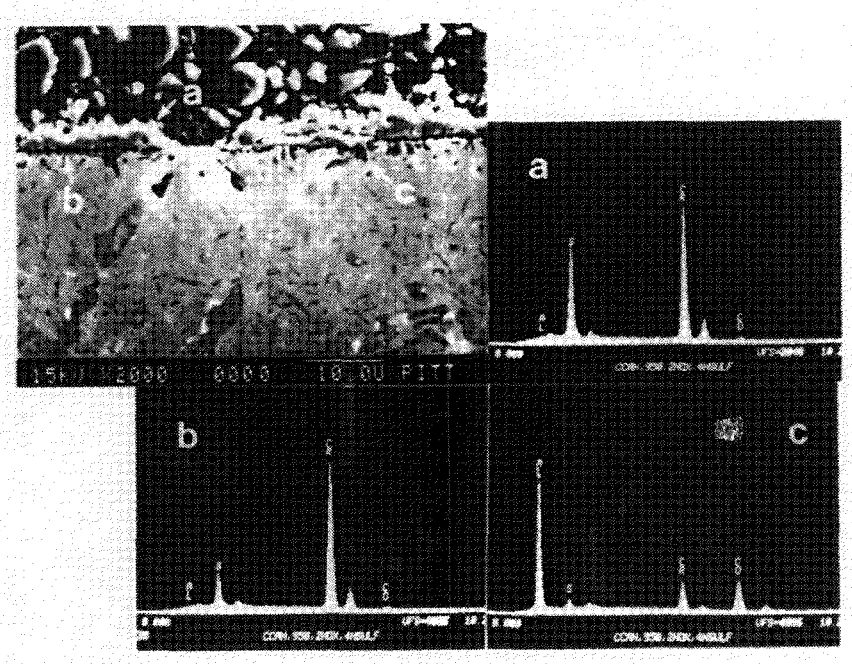

Figure 25: Co-18Cr-6Al-1Hf exposed to a H_2/H_2O gas mixture for 2 hours and subsequently exposed to a $H_2/H_2S/H_2O$ gas mixture for 4 hours at 950°C.

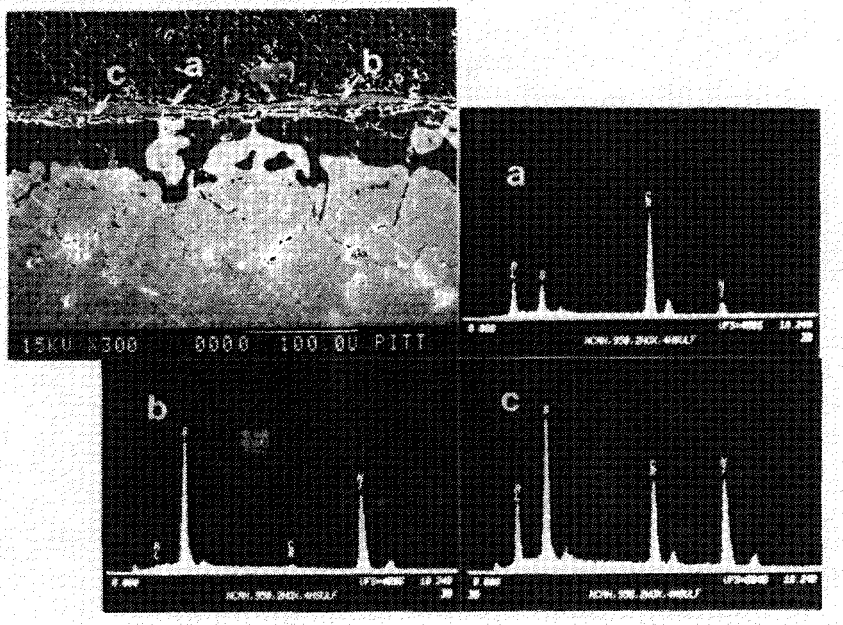

Figure 26: Ni-18Cr-6Al-1Hf exposed to a H_2/H_2O gas mixture for 2 hours and subsequently exposed to a $H_2/H_2S/H_2O$ gas mixture for 4 hours at 950°C.

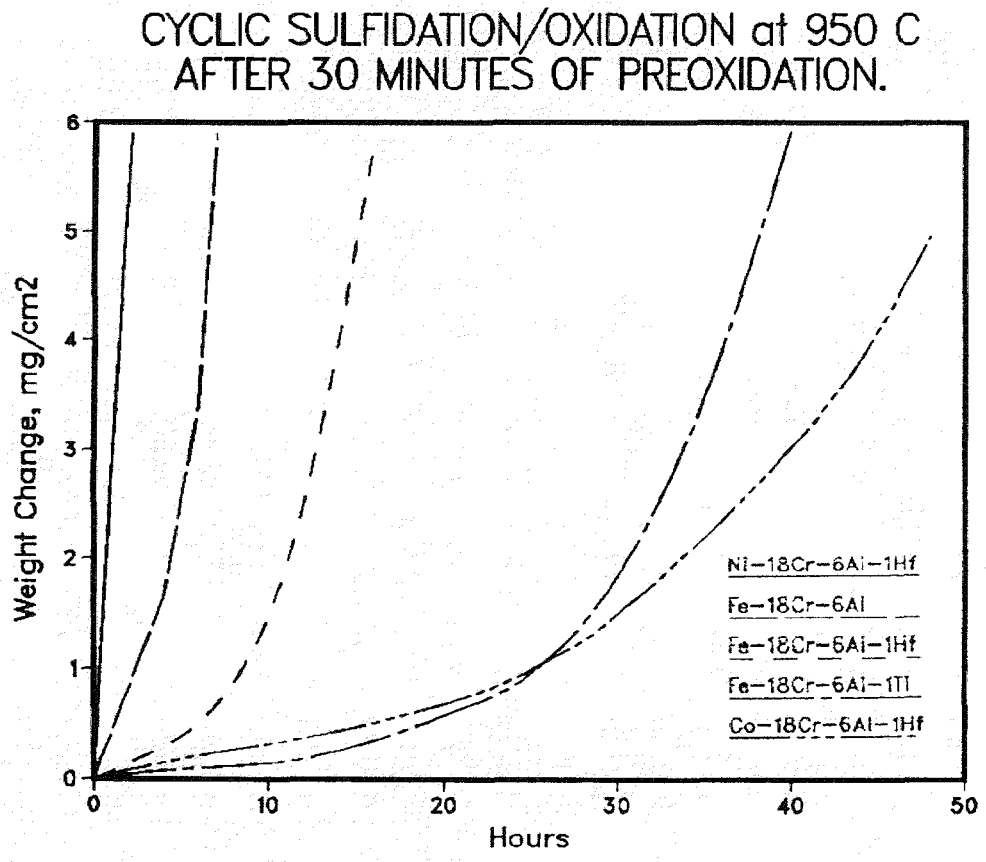

Figure 27: Weight changes vs. time for cyclic sulfidation/oxidation (4 hour cycles) in a $H_2/H_2S/H_2O$ gas mixture after preoxidation in a H_2/H_2O gas mixture for 30 minutes at 950°C.

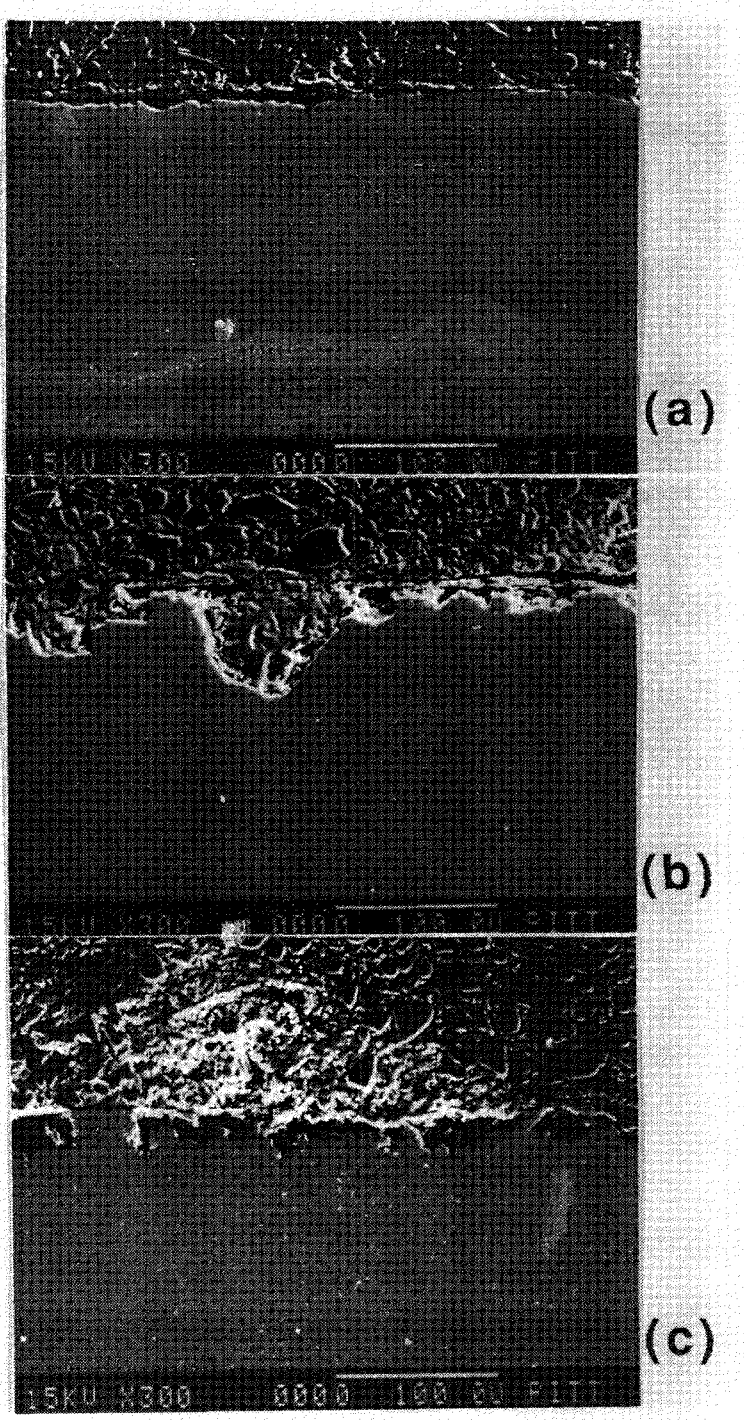

Figure 28: Cross-sections of (a) Fe-Cr-Al-Ti, (b) Fe-Cr-Al-Hf, and (c) Co-Cr-Al-Hf after 995 hrs. exposure in a syngas atmosphere at 550°c.

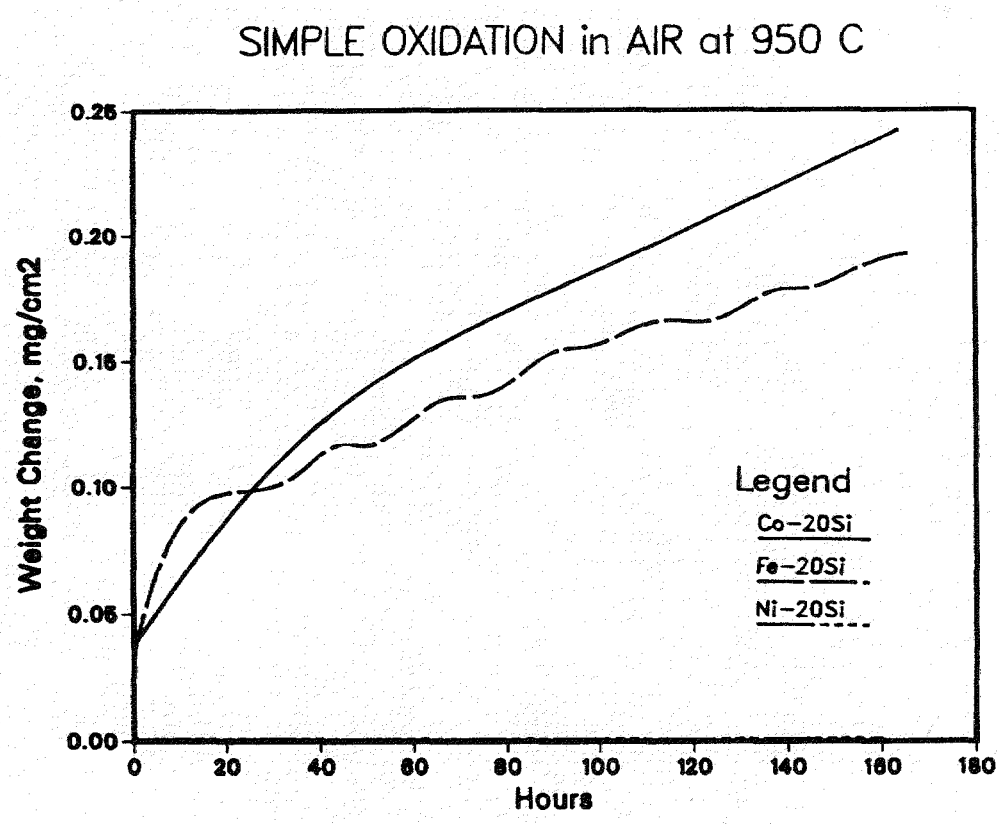

Figure 29: Weight changes vs. time for the alloys during oxidation in air at 950°C.

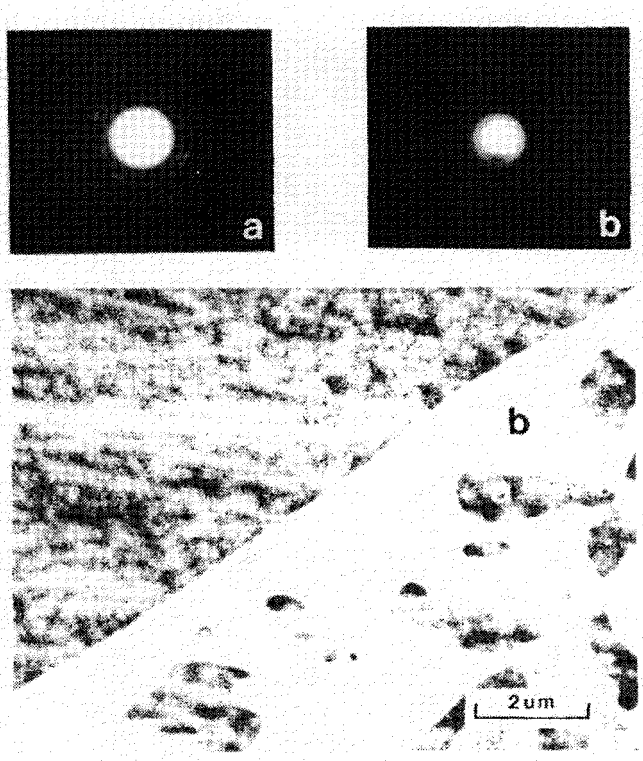

Figure 30: TEM micrograph of Ni-20Si oxidized in air at 950°C for an hour with selected area diffraction patterns.

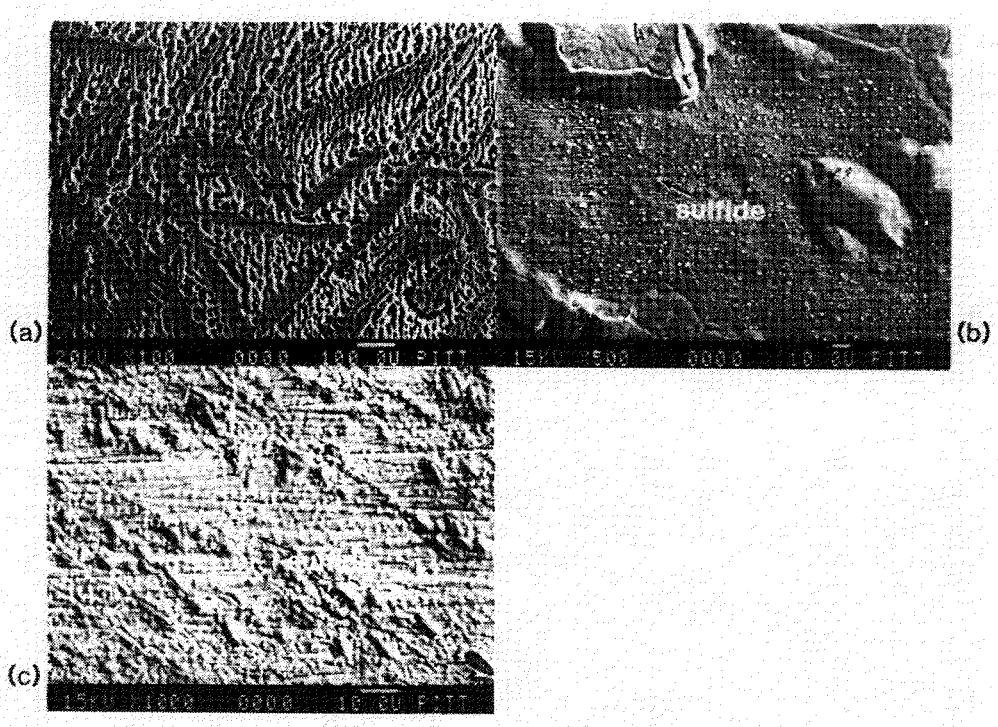

Figure 31: Silica forming alloys sulfidized in a H_2/H_2S gas mixture at 950°C for 4 hours. (a) Ni-20Si (b) Fe-20Si and (C) Co-20Si.

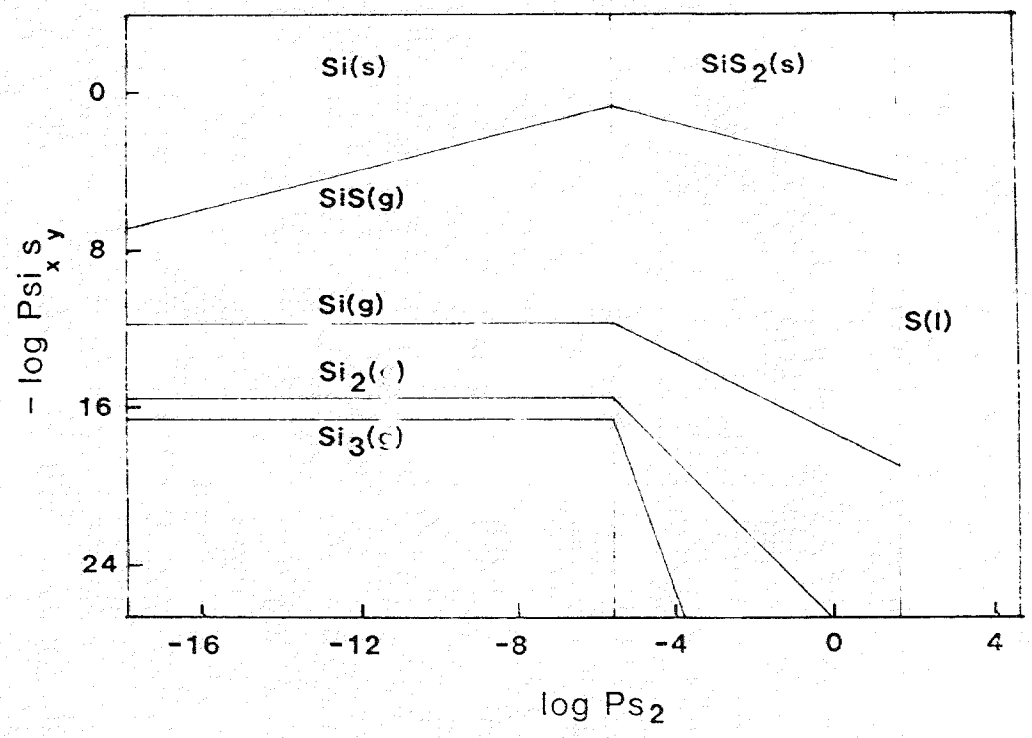

Figure 32: Vapor species diagram for the Si-S system at 950°C.

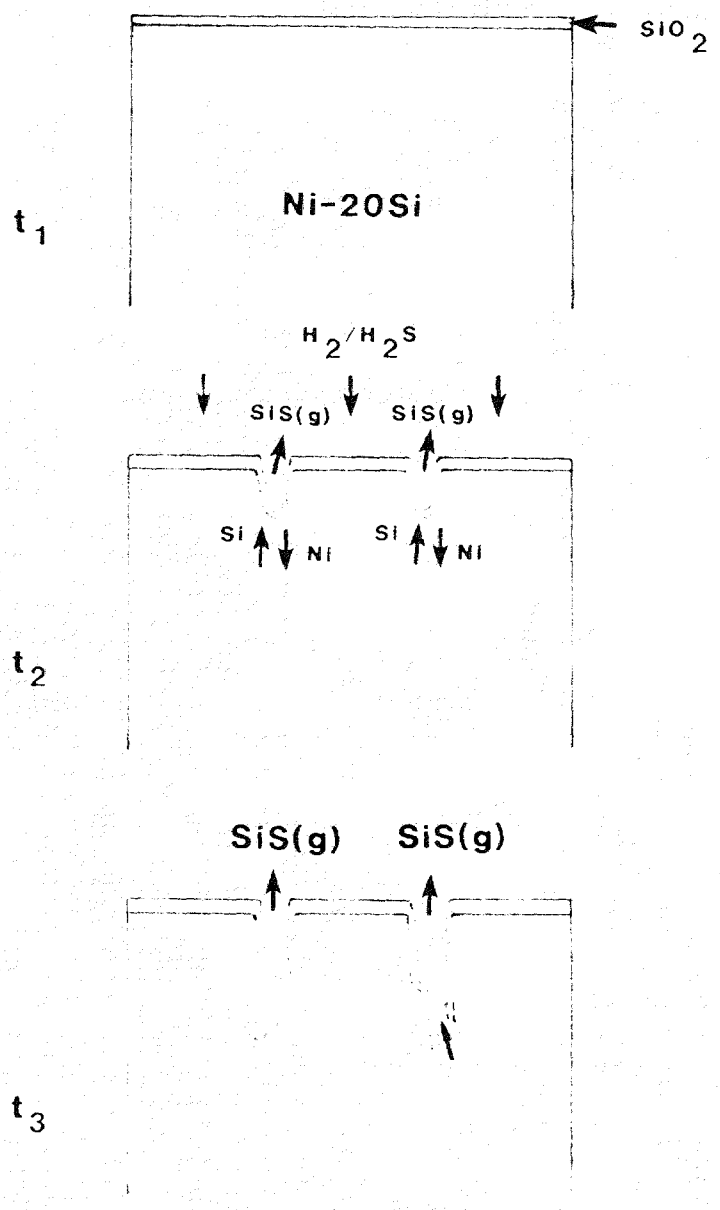

Figure 33: Schematic representation of degradation of Ni-20Si in a H_2/H_2S gas mixture at 950°C.

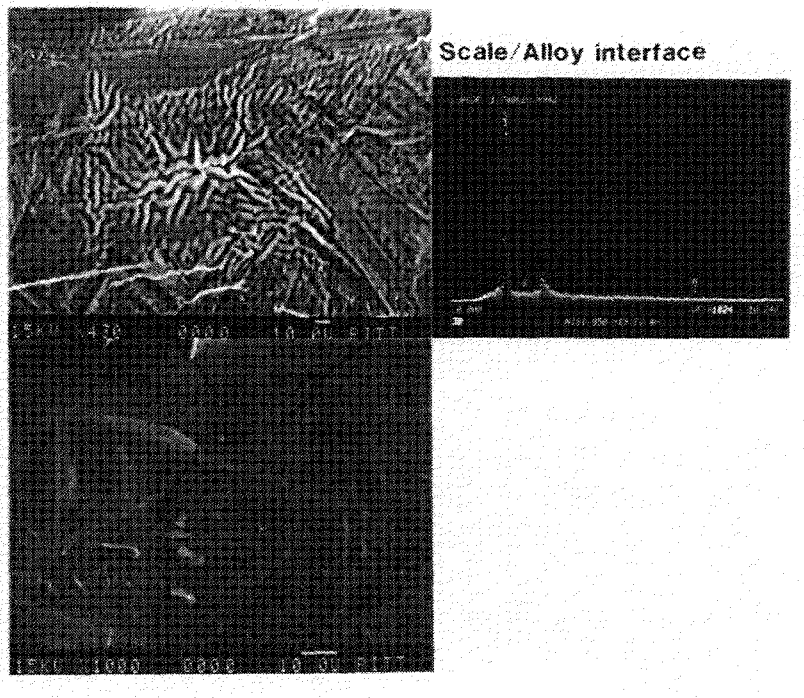

Figure 34: Ni-20Si exposed to a H_2/H_2O gas mixture for 30 minutes and subsequently exposed to a $H_2/H_2O/H_2S$ gas mixture for 4 hours at 950°C.

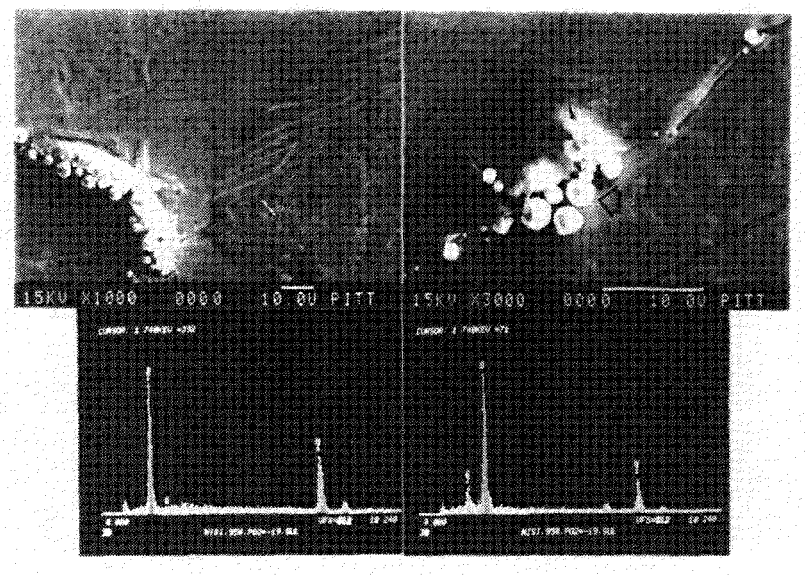

Figure 35: Ni-20Si exposed to a H_2/H_2O gas mixture for 30 minutes and subsequently exposed to a $H_2/H_2O/H_2S$ gas mixture for 4 hours at 950°C.

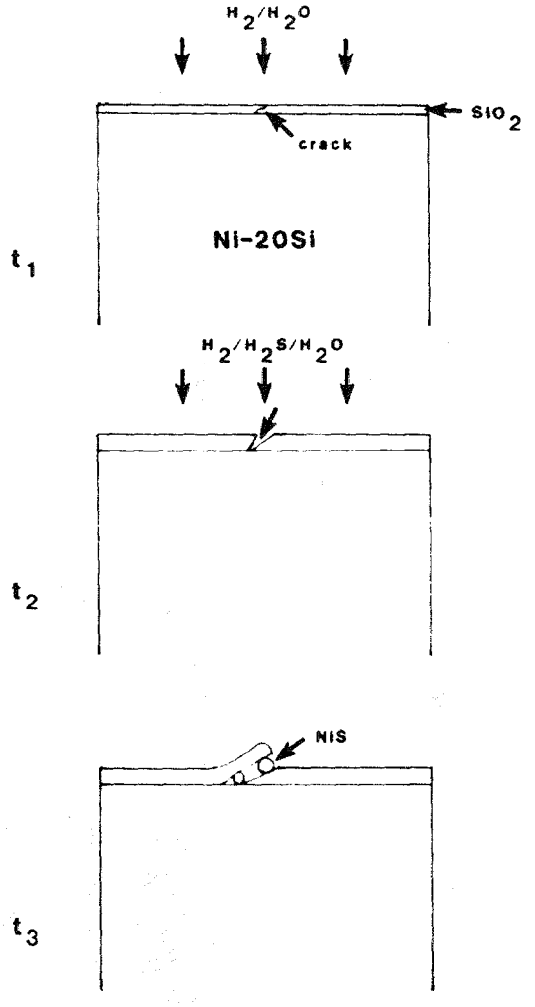

Figure 36: Schematic representation of the breakdown of preformed SiO_2 scale formed on Ni-20Si by sulfur-bearing gases.

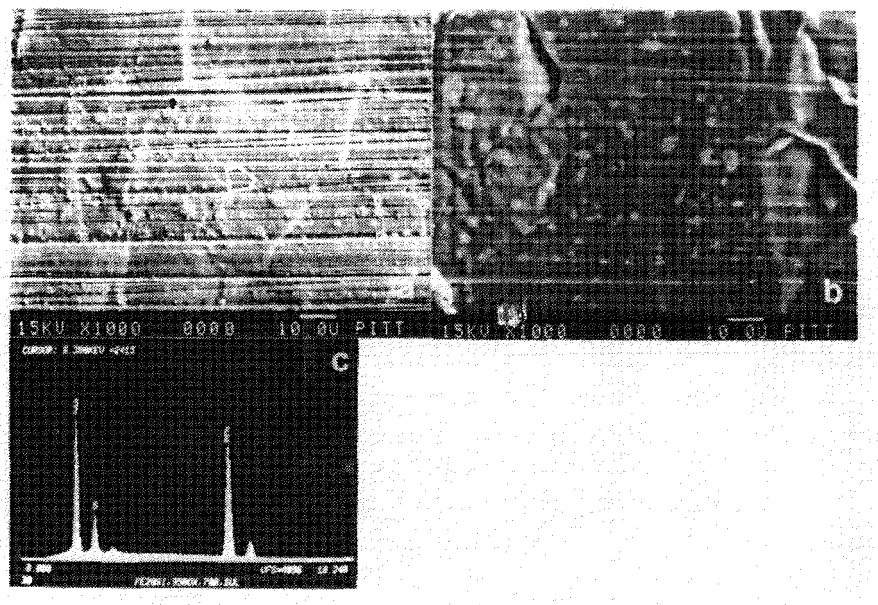

Figure 37: Fe-20Si exposed to a H_2/H_2O gas mixture or 30 minutes and subsequently exposed to a $H_2/H_2O/H_2S$ gas mixture for 4 hours at 700°C. (a) external oxide scale (b) underside of the oxide scale.

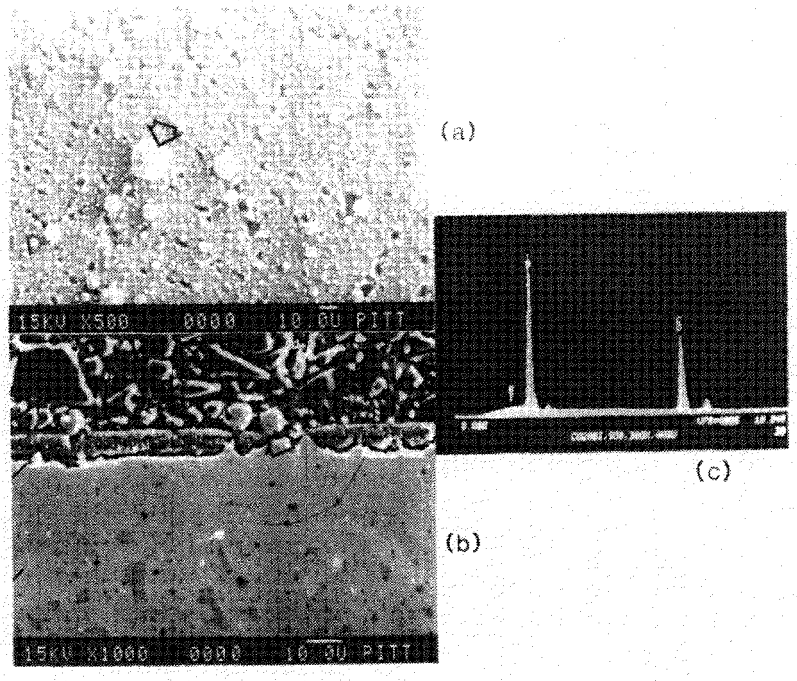

Figure 38: Co-20Si exposed to a H_2/H_2O gas mixture for 30 minutes and subsequently exposed to a $H_2/H_2O/H_2S$ gas mixture for 4 hours at 950°C. (a) external oxide scale, (b) cross section of (a), and (c) EDX spectra of sulfide(arrow).

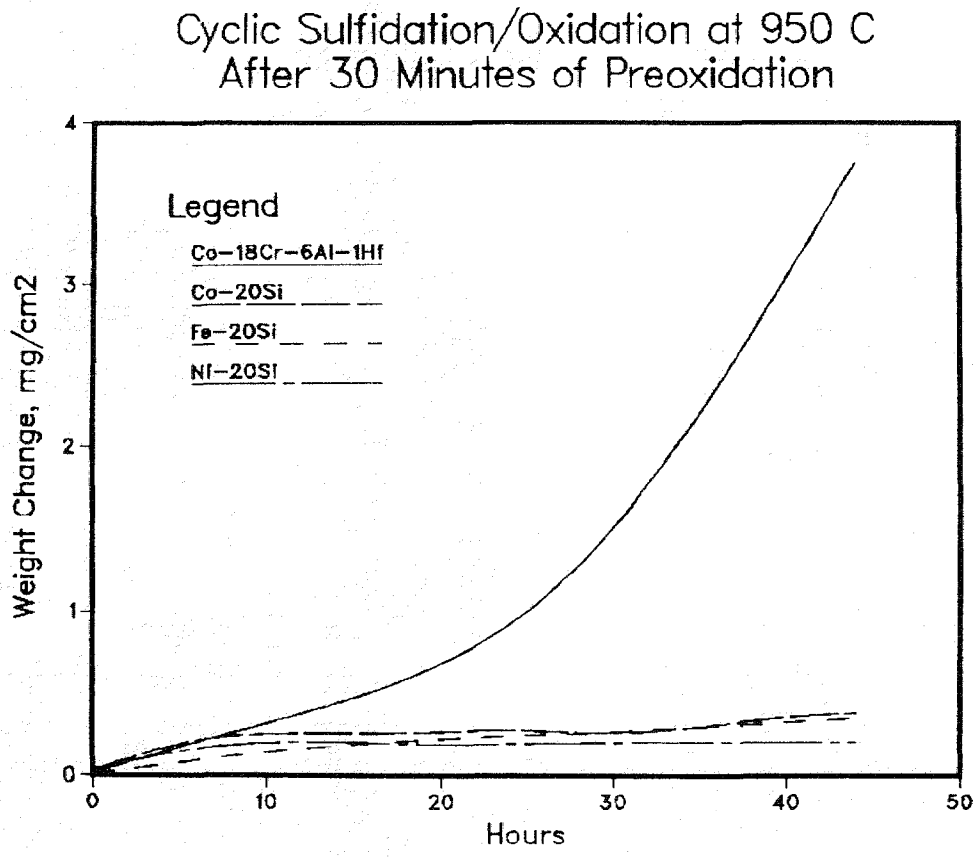

Figure 39: Weight changes vs. time for cyclic sulfidation/oxidation (4 hour cycles) in a $H_2/H_2S/H_2O$ gas mixture after preoxidation in a H_2/H_2O gas mixture for 30 minutes at 950°C.

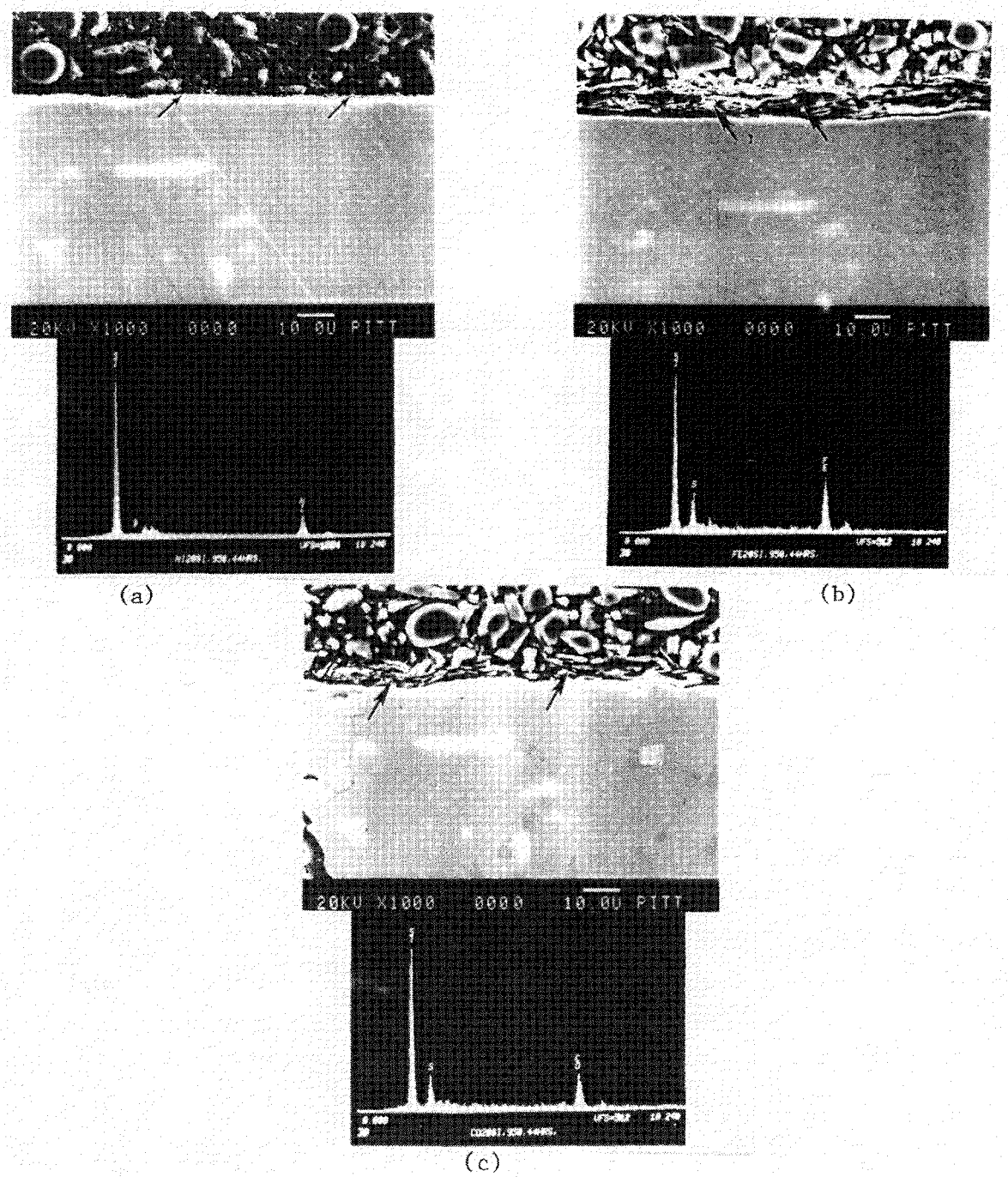

Figure 40: Transverse sections of specimens after 44 hours of cyclic sulfidation/oxidation (4 hour cycle) in a $H_2/H_2S/H_2O$ gas mixture after preoxidation in a H_2/H_2O gas mixture for 30 minutes at 950°C. (a) Ni-20Si, (b) Fe-20Si and (c) Co-20Si.

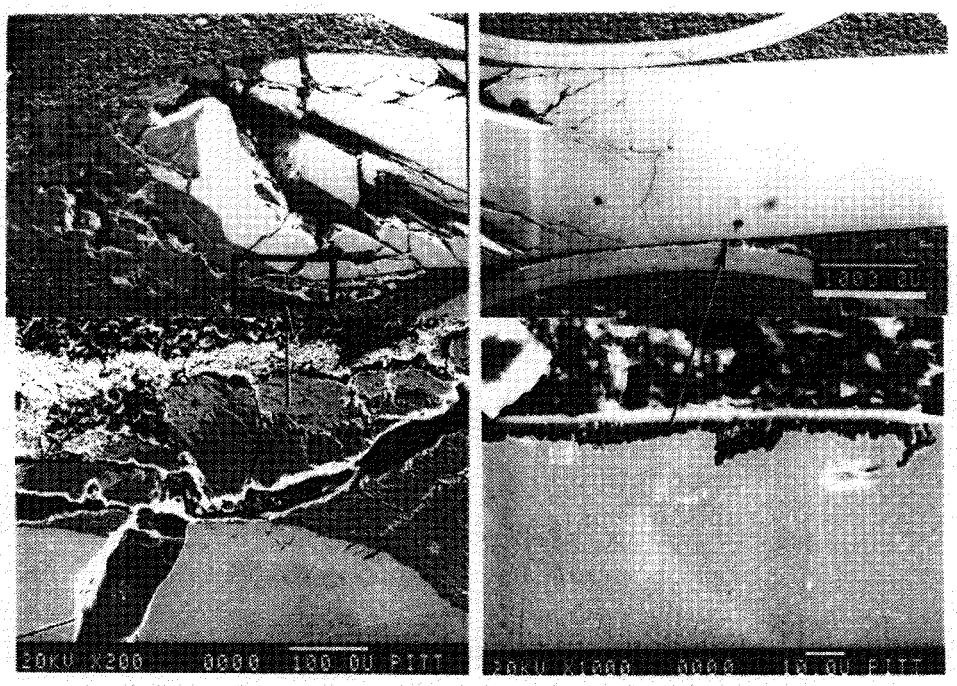

Figure 41: Ni-20Si which was coated with gasifier slag and then exposed to syngas at 550°C for 160 hours. These show two different degradation areas. (a) Severely degraded area and (b) protective area.

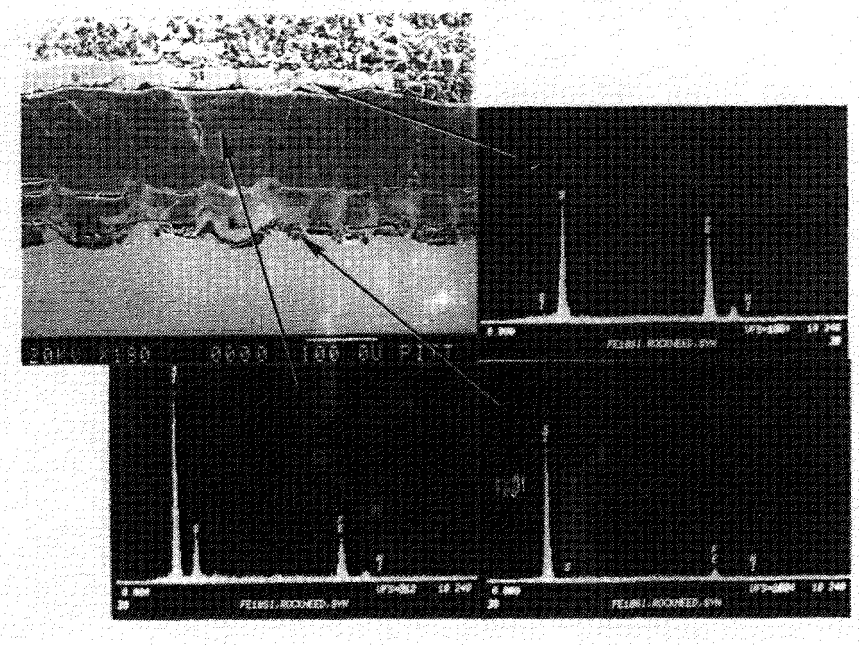

Figure 42: Fe-20Si which was coated with gasifier slag and then exposed to syngas at 550°C for 160 hours.